Talbot, H., Bischoff, J., Inglis, G. N., Collinson, M., & Pancost, R. D. (2016). Polyfunctionalised bio- and geohopanoids in the Eocene Cobham Lignite. *Organic Geochemistry*, *96*, 77-92. https://doi.org/10.1016/j.orggeochem.2016.03.006

Polyfunctionalised bio- and geohopanoids in the Eocene Cobham Lignite

Helen M. Talbot[a,*], Juliane Bischoff[a], Gordon N. Inglis[b], Margaret E. Collinson[c] and Richard D. Pancost[b]

[a]*School of Civil Engineering and Geosciences, Newcastle University, Newcastle upon Tyne, NE1 7RU, UK.*

[b]*Organic Geochemistry Unit, The Cabot Institute and Bristol Biogeochemistry Research Centre, School of Chemistry, University of Bristol, Bristol BS8 1TS, UK.*

[c]*Department of Earth Sciences, Royal Holloway University of London, Egham, Surrey TW20 0EX, UK.*

Keywords: Cobham Lignite, peat, PETM, methanotrophy, bacteriohopanepolyols, aminobacteriohopanepentol, anhydrobacteriohopanetetrol

* *Corresponding author. Tel.: +44 (0)191 208 6426*

E-mail address: helen.talbot@ncl.ac.uk (H. M. Talbot).

Abstract

We investigated the bacteriohopanepolyol (BHP) distribution in the Cobham Lignite sequence (SE England) deposited across the Palaeocene-Eocene boundary including part of the Palaeocene-Eocene Thermal Maximum (PETM) as shown previously by a negative carbon isotope excursion (CIE). A variety of BHPs were identified, including the commonly occurring and non-source specific biohopanoid bacteriohopanetetrol (BHT) and 32,35-anhydroBHT which was the most abundant polyfunctionalised geohopanoid in the majority of samples. BHPs with a terminal amine functionality, diagnostic biomarkers for methanotrophic bacteria were identified throughout the sequence, with similar distributions in both the lower laminated and upper blocky lignite except that 35-aminobacteriohopanepentol (aminopentol) indicative of Type I methanotrophs (gammaproteobacteria) was generally more abundant in the upper section within the CIE.

The diagenetic fate of these compounds is currently poorly constrained, however, we also identified the recently reported N-containing transformation product anhydroaminotriol and several tentatively assigned novel N-containing structures potentially containing ketone functionalities. Although present throughout the section, there is a sharp peak in the occurrence of these novel compounds correlated with the onset of the CIE and highly isotopically depleted hopanes in the upper part of the laminated lignite, both also correlate well with peak abundance of aminopentol. The significant abundance of these compounds suggests that 35-amino BHPs have their own specific diagenetic pathway, potentially providing an alternative method allowing methanotroph activity to be traced in older samples even if the original biohopanoid markers are no longer present.

At this time we cannot preclude the possibility that some or all of these BHPs have been produced by more recent subsurface activity, post deposition of the lignite to date; however, that would not be expected to generate the observed stratigraphic variability and we suggest that unprecedented observations of a range of highly functionalised biohopanoids in samples of this age could significantly extend the window of their known occurrence.

1. Introduction

Bacteriohopanepolyols (BHPs) are highly functionalised pentacyclic triterpenoids derived from a wide range of prokaryotes (e.g. Rohmer et al., 1984; Pearson et al., 2007, 2009). In their biological form (i.e. biohopanoids), they comprise a diverse suite of structures (e.g. Rohmer, 1993; See Appendix for examples) which have been linked to cellular membrane adaptation, regulating fluidity and permeability in response to environmental stress (e.g. Kannenberg and Poralla, 1999; Welander et al., 2009; Sáenz et al., 2012; Kulkarni et al., 2013). Typically they contain four, five or six functional groups (termed tetra-, penta- and hexafunctionalised respectively) at the C-30 to 35 positions of the side chain although cyclised side chains are also known. For example, adenosylhopane (**Ip**) is the precursor for all other side chain extended BHPs (Bradley et al., 2010) via a pathway involving the intermediate ribosylhopane (Liu et al., 2014; Bodlenner et al., 2015). Biohopanoids are also the precursors of the ubiquitous geohopanoids (hopanols, hopanoic acids, hopanes) found in geological materials (e.g. Ourisson et al., 1987; Ourisson and Albrecht, 1992; Farrimond et al., 2004).

Biohopanoids can provide useful information about certain source organisms, biogeochemical processes and environmental conditions (e.g. Talbot and Farrimond, 2007). One such group are BHPs with an amine functionality at the C-35 position (collectively termed aminoBHPs herein; e.g. Talbot et al., 2014; Wagner et al., 2014; Spencer-Jones et al., 2015) which include 35-aminobacteriohopane-32,33,34-triol (aminotriol from herein, **If**), 35-aminobacteriohopane-31,32,33,34-tetrol (aminotetrol, **Ig**) and 35-aminobacteriohopane-30,31,32,33,34-pentol (aminopentol, **Ih**). Sources of aminopentol are thought to be restricted to Type I aerobic methane oxidising bacteria (Gammaproteobacteria; e.g. Neunlist and Rohmer, 1985; Cvejic et al., 2000; van Winden et al., 2012a), whilst aminotetrol is produced

by both Type I and II (Alphaproteobacteria) methanotrophs. The only known additional source of the penta- and hexafunctioanlised compounds are some species of *Desulfovibrio* sulphate reducing bacteria (SRB; Blumenberg et al., 2006, 2009), although aminopentol was only reported from one species at trace levels (Blumenberg et al., 2012). Further, when observed in *Desulfovibrio* sp., the ratio of aminotriol to aminotetrol (**If/Ig**) was in the range of 20 to 100 (Blumenberg et al., 2006, 2009, 2012) whilst it is significantly lower in most methanotrophs, with the pentafunctionalised compound often more abundant (e.g. Janke et al., 1999; Talbot et al., 2001). Aminotriol is less diagnostic as it is produced by a range of other prokaryotes (including other proteobacteria and some cyanobacteria; Talbot et al., 2008 and references therein) in addition to all Type II and some Type I methanotrophs (Talbot et al., 2001; van Winden et al., 2012a; Banta et al., 2015).

AminoBHPs have been reported from a wide range of environments including soils (e.g. Cooke et al., 2008a; Xu et al., 2009; Pearson et al., 2009; Rethemeyer et al., 2010; Kim et al., 2011; Zhu et al., 2011), peats (e.g. van Winden et al., 2012a,b), marine, river and lacustrine sediments (e.g. Talbot et al., 2003a; Talbot and Farrimond, 2007; Coolen et al., 2008; Blumenberg et al., 2010; Zhu et al., 2010, 2011; Blumenberg et al., 2013). Aminotetrol (**Ig**) and aminopentol (**Ih**) are therefore of particular interest and have been used to identify material sourced from sites of intense aerobic methane oxidation such as river estuaries (Zhu et al., 2010), tropical wetlands (Talbot et al., 2014; Wagner et al., 2014; Spencer-Jones et al., 2015) and water columns (e.g. Blumenberg et al., 2007; Wakeham et al., 2007; Berndmeyer et al., 2013). Other markers for Type I aerobic methanotrophs include hopanoids methylated at the C-3 position (e.g. Cvejic et al., 2000), but non-methanotrophs can also be potential sources of this structural feature (e.g. Welander and Summons, 2012). Typically therefore, these studies also rely on analysis of compound specific carbon isotope ratios with strong isotopic depletion expected for methanotroph-derived lipids (e.g. Collister et al., 1992). However, the absence of C-3 methylated pseudohomologues of these aminoBHP compounds does not preclude either the Type II methanotrophs or Type I

organisms such as *Methylomonas* sp. or *Methylovulum* sp. (e.g. Rohmer et al., 1984; van Winden et al., 2012a) which do not produce the methylated homologues (see discussion in Talbot et al., 2014).

Originally considered to be rapidly transformed to geohopanoids at the earliest stages of diagenesis (both free and bound), evidence is now growing that polyfunctionalised biohopanoids may be more stable than originally thought. The oldest reported polyfunctionalised biohopanoid is bacteriohopane-32,33,34,35-tetrol (BHT; **Ic**) in a sample of marine Palaeogene cores from Tanzania dating to 50.4-49.7 million years ago (Ma; van Dongen et al., 2006). This compound is the most frequently reported BHP structure, facilitated by the fact that it is amenable to analysis by gas chromatography mass spectrometry (GCMS) as well as liquid chromatography mass spectrometry (LCMS; e.g. Talbot et al., 2003a). It has a wide range of potential prokaryotic sources meaning that it cannot be considered as indicative of any particular group of bacteria or set of environmental conditions (e.g. Talbot et al., 2008). Additional early degradation products retaining multiple functional groups derived from BHT or more complex precursors such as BHT cyclitol ether (**Im**) or BHT glucosamine (**In**) include 32,35-anhydrobacteriohopane-32,33,34,35-tetrol (anhydroBHT; **Ia**) and its C-2 methylated homologue (**IIa**; Schaeffer et al., 2008, 2010) and they have been reported in samples up to Jurassic in age (Bednarczyk et al., 2005). Multiple isomers of the related compound derived from a pentafunctionalised precursor i.e. anhydrobacteriohopanepentol (anhydroBHPentol; **Id**) have been reported from geothermal sinters (Talbot et al., 2005; Gibson et al., 2014).

Recently we have identified aminoBHPs including aminopentol (**Ih**) in samples from the Congo deep-sea fan aged up to 1.2 Ma and the source of the material is proposed as continental wetland environments (Talbot et al., 2014; Spencer-Jones et al., 2015; Spencer-Jones, 2016). Burhan et al. (2002) reported aminotriol from the Be'eri sulfur deposit (Pleistocene age sandstones of the Southwestern Mediterranean Coastal Plain of Israel),

however, it is uncertain if it represents a Pleistocene age signal or one from sub-contemporary bacteria feeding on seeping methane. These findings suggest that BHP compounds produced in aerobic systems can be preserved in the geological record when conditions are favourable and could therefore be useful in examining methane cycling in more ancient settings.

To explore the potential for BHP preservation in ancient sediments, we investigated the BHP signature of a well preserved, immature lignite sequence from southern England. The Cobham Lignite is an exceptional example of a terrestrial lacustrine/mire deposit associated with the Palaeocene-Eocene thermal maximum (PETM; Collinson et al., 2003, 2007, 2009). Previously, a negative carbon isotope excursion (CIE) indicated by a sharp depletion in $\delta^{13}C$ of ~1 ‰ in the bulk organic carbon within the section has been interpreted as being the negative CIE characteristic of the PETM onset, although its magnitude is markedly lower than the total extent of the CIE observed in other terrestrial settings (McInerney and Wing, 2011). Furthermore, isotopically light hopanoids have also been reported from this section, suggesting an increase in the methanotroph population resulting from enhanced methane production, likely driven by hydrological changes towards a warmer and wetter climate (Pancost et al., 2007). These changes are also manifested as a lithological change from laminated to blocky lignite. Hopanoids at this site are present in exceptional abundance relative to other biomarkers and are relatively immature based on observation of the biological 17β,21β(*H*) configuration and lack of compounds with 22*S* stereochemistry (Pancost et al., 2007). We therefore considered this site favourable for investigation of the potential for preservation of polyfunctionalised biohopanoids.

2. Methods

2.1 Site and samples

The ca. 2 m thick early Paleogene Cobham Lignite sequence used for this study was sampled from a temporary exposure, which became available near Cobham, Kent, southern England, when a cutting was made through a hill for construction of the Channel Tunnel Rail Link during 1999-2000. In order to procure a complete sequence of the lignite with intact stratigraphy, surrounding sediment was excavated to produce pillars (10-15 cm in depth and width) free on three sides. The three exposed sides were enclosed in a plaster jacket to prevent breakage and pillars were removed from the exposure at the fourth side using spades. The fourth side was not enclosed. These plaster-jacketed pillars were stored in ambient room conditions whilst attempts were made to obtain funding for their study.

Prior to sub-sampling sediment was removed and discarded from the surface of the exposed side to a depth of c. 3 cm until sediment with original appearance (e.g. colour, degree of integrity) was reached. Sub-sampling of each cleaned pillar was completed within one day. Cleaning and sub-sampling was undertaken using sharp single-edged razor blades that had been rinsed in alcohol and treated in a furnace prior to use. A fresh razor blade was used for each sub-sample. Sub-samples specifically for geochemical analysis were taken from near the centre of the pillar, avoiding the sides. These samples were dried and individually wrapped in aluminium foil, which had previously been treated in a furnace, then transported to the University of Bristol for extraction. The current study utilised aliquots of total lipid extract (TLE) originally prepared by Pancost et al. (2007) and which had been stored dry and frozen (-20°C) until transported to Newcastle in 2012 for BHP analysis.

The Cobham Lignite sequence is underlain by a sand and mud unit, beneath which is the late Paleocene Upnor Formation (shallow marine). The Early Eocene Woolwich Shell Beds (marginal marine/lagoonal) overly the lignite. The Woolwich Shell Beds contain the *Apectodinium* acme (Collinson et al., 2009), thus, in combination with the CIE in the upper part of the lower laminated lignite (Pancost et al., 2007), demonstrate that all of the blocky lignite is within the PETM and probably in the early part of the PETM (Collinson et al., 2009).

190 The site, stratigraphy, lithology, palynology, vegetation change and wetland plant
191 mesofossils have been described in detail elsewhere (Table 1; Collinson et al., 2003, 2007,
192 2009, 2013; Steart et al., 2007).
193
194 The Cobham Lignite sequence includes two thick units of lignite and two thin clay layers. A
195 basal thin pale clay layer (3 cm thick) underlies the lower laminated lignite unit (up to 55 cm
196 thick). The uppermost 25 mm of the lower laminated lignite is transitional and contains thin
197 clay laminae (upper part of Figure 3.3 in Steart et al., 2007). A thicker (up to 10 cm) pale clay
198 layer separates the laminated lignite from the overlying blocky lignite unit (up to 132 cm
199 thick). The bottom of the basal thin pale clay layer is set to 0 cm for the section (Table 1). In
200 total thirty five samples from the original set described by Pancost et al. (2007) were chosen
201 for BHP analysis. The samples ranged from the underlying sand and mud unit through the
202 laminated lignite, middle clay and blocky lignite including samples from the onset of the CIE
203 in the upper laminated lignite (Table 1).
204
205 *2.2 Extraction and derivatisation*
206 Prior to lipid extraction samples were powdered with a mortar and pestle. The powdered
207 samples were extracted by sonication with a sequence of increasingly polar solvents (four
208 times with dichloromethane (DCM), four times with DCM/methanol (1:1 v/v) and three times
209 with methanol) to produce a total lipid extract (TLE; Pancost et al., 2007).
210
211 An aliquot of each TLE was acetylated by adding acetic anhydride and pyridine (1 ml each)
212 and heating at 50 °C for 1 h then left at room temperature overnight to yield acetylated
213 BHPs. The acetic anhydride and pyridine were removed under a stream of N_2. The resulting
214 acetylated extract was dissolved in MeOH/propan-2-ol (3:2, v/v) and filtered through a 0.45
215 micron PTFE filter, blown down to dryness and redissolved in 500 μl MeOH/propan-2-ol (3:2,
216 v/v) for analysis. Sessions et al. (2013) showed using GCMS analysis that acetylation of

hopanoids can produce anhydroBHT if run for more than 15-30 minutes. However, similar tests on a range of acetylation reagent volumes and reaction times showed no statistically significant variation in concentration or production of anhydroBHT on samples analysed by ion-trap LCMS (Spencer-Jones, 2016).

As no standards were added prior to splitting of the TLE and derivatisation, only relative abundances within individual samples are reported below and are based on LCMS data only.

2.3 Analytical HPLC-APCI-MS

BHPs were measured using reversed-phase HPLC-APCI-MS as described previously (e.g. Cooke et al., 2008a; van Winden et al., 2012a). Compounds were separated using a Thermo Finnigan Surveyor HPLC system equipped with a Phenomenex Gemini C18 5 µm column (150 mm x 3.0 mm i.d.) and a security guard column of the same material. The flow rate was 0.5 ml/min at 30 °C with the following gradient: 90% A and 10% B (0 min); 59% A, 1% B and 40% C (at 25 min); isocratic (to 40 min), returning to starting conditions over 5 min and stabilizing for 15 min, with A = MeOH, B = water and C = propan-2-ol (all Fisher HPLC grade). The HPLC system was connected to a Thermo Finnigan LCQ ion trap MS instrument equipped with an APCI source operated in positive ion mode. Settings were: capillary temperature 155 °C, APCI vaporiser temperature 400 °C, corona discharge current 8 µA, sheath gas flow 40 and auxiliary gas 10 (arbitrary units). The instrument was tuned as described previously (Talbot et al., 2003b,c). Detection was achieved at an isolation width of *m/z* 4.0 and fragmentation with normalised collisional dissociation energy of 30% and an activation Q value (parameter determining the m/z range of the observed fragment ions) of 0.15. $LCMS^n$ was carried out in data-dependent mode with three scan events: SCAN 1 – full mass spectrum, range m/z 300–1300; SCAN 2: data-dependent MS^2 spectrum of the most

intense ion from SCAN 1; SCAN 3: data-dependent MS^3 spectrum of the most intense ion from SCAN 2.

For standard runs dynamic exclusion was turned on limiting the number of MS^2 scans per individual parent ion to 3 before automatically switching to the next most abundant ion. Where necessary, additional targeted analyses were performed to increase the number of MS^2 scans per peak. Structures were assigned from comparison with published spectra where possible (Talbot et al., 2003b,c, 2005, 2007a,b) or by comparison of their APCI spectra with those of known compounds as described below.

Although full quantification was not possible, we applied the usual response factors determined previously for BHPs with and without nitrogen where N-containing compounds give an average relative response 1.5 times that of BHPs without a N atom (see van Winden et al., 2012a for details). Furthermore, co elution of aminotriol (**If**) and anhydroaminotriol (**Ii**) complicates the identification and assessment of the anhydroaminotriol peak area. Anhydroaminotriol has a base peak $[M+H]^+$ of m/z 654. Aminotriol has $[M+H]^+$ of m/z 714 but also produces some m/z 654 as well via loss of 1 acetylated functional group (CH_3COOH) which is also seen in the full mass spectrum (SCAN 1). Therefore even when only aminotriol is present there will still be a minor m/z 654 peak. To minimise this effect (i.e. minimise any overestimation of anhydroaminotriol) the relative areas of the m/z 714 and 654 peak in all samples where both are present were compared (Table 1; Column **If/Ii**). The lowest relative amount of the 654 peak in any sample is equal to 17.9% of the 714 peak area. Therefore 17.9% of the corresponding 714 peak area was subtracted from the m/z 654 peak for each individual sample. The reduced value for the m/z 654 was then used in the calculation of the relative abundance of anhydroaminotriol as a proportion of total BHPs (Table 1).

2.4 GC-MS Analysis

Acetylated hopanepolyols, dissolved in DCM, were analysed by GC-MS using an Agilent 7890A GC split/splitless injector (300°C) linked to an Agilent 5975C MSD (electron energy 70 eV; filament current 220 mA; source temperature 230°C; multiplier voltage 2000V; interface temperature 350°C). A 15 m DB5-HT fused silica column (0.25 mm i.d.; 0.1 mm film thickness) was used with helium as the carrier gas. The oven temperature was programmed from 50 to 200°C at 15°C/min (held for 1 min), from 200 to 250°C at 10 °C/min (held for 1 min) and from 250 to 350°C at 5°C/min (held for 8 min; Talbot et al., 2003a). Hopanoids were identified from full scan (m/z 50–750) analysis of selected samples, by comparison with authentic standards and published spectra and by relative retention times. Additionally, one sample (11.95 cm; Table 1) was analysed in SIM mode targeting ions m/z 191, 205, 391, 405, 449, 493 and 507 (see below).

3. Results

3.1. Identification of polyfunctionalised hopanoids in the Cobham lignite

3.1.1. Biohopanoids

Bacteriohopanetetrol (BHT; **Ic**) was present in 26 of the 35 samples and was the only biohopanoid observed in any of the Cobham lignite samples which did not contain an amine at the C-35 position (Fig.1a, b for example; Table 1). Most samples also contained the common tetrafunctionalised aminotriol (**If**), typically accompanied by similar relative amounts of the pentafunctionalised aminotetrol (**Ig**) (Fig. 2 for example; Table 1). In a smaller number of samples, the hexafunctionalised aminopentol (**Ih**, Fig. 2; Table 1) was also observed. These compounds were identified by relative retention time (Fig. 2) and interpretation of APCI mass spectra in comparison to previously published data (Talbot et al., 2003b,c).

3.1.2 AnhydroBHT and related novel hopanoids

298 The common BHP transformation product anhydroBHT (**Ia**) was present in all but one
299 sample and was frequently the most abundant BHP present (Table 1). It is readily identified
300 in the diacetate form via EI mass spectrometry (peak **Ia**, Figs. 1b, 3a). Although this
301 spectrum has been published previously (e.g. Bednarczyk et al., 2005), it is included to allow
302 for comparison with a group of related novel components described here for the first time
303 (Fig. 3a).
304
305 When analysed by reversed phase HPLC, diacetylated anhydroBHT (**Ia**) elutes later than
306 BHT (**Ic**), and has an APCI base peak ion of *m/z* 613 (= $[M+H]^+$; Fig. 1a). The MS^2 spectrum
307 (Fig. 3b; cf. Talbot et al., 2005) includes major fragments of *m/z* 553 and 493 indicating 2
308 neutral losses of 60 Da (i.e. the acetylated OH groups at C-33 and C-34 [CH_3COOH]) and
309 ion *m/z* 475 indicates loss of 18 Da (loss of the heterocyclic oxygen as H_2O). Lower intensity
310 ions indicating a 2nd pathway of initial loss of 18 Da followed by 2 losses of 60 Da are also
311 present (*m/z* 595, 535 and 475 respectively). There are also characteristic ions more directly
312 indicative of the hopanoid nature of the compounds at *m/z* 191 as seen in the EI spectrum
313 and at *m/z* 421 indicating neutral loss of the A+B rings from the protonated molecule. Low
314 levels of a second, earlier eluting isomer (**Ia'**; possibly the α,β isomer e.g. Eickhoff et al.,
315 2014) were also present in some samples (Fig. 1a, Table 1).
316
317 In many samples, another peak (**Ib**, Fig. 1a) was observed eluting just after anhydroBHT (**Ia**)
318 with a base peak ion of *m/z* 627, potentially indicating a methylated pseudohomologue of
319 anhydroBHT. Based on the retention time this peak was anticipated to be the C-2
320 methylated homologue as the C-3 compound would elute later during both LCMS and
321 GCMS analysis (e.g. Talbot et al., 2003; Farrimond et al., 2004), however, the expected *m/z*
322 205 ion (indicating methylation on the A+B rings) was not present (or only at very low
323 relative abundance, see below) in the APCI MS^2 spectrum (Fig. 3d). An ion of *m/z* 191 was
324 present suggesting instead an additional CH_2 located at a position other than on the A/B
325 rings. Two ions indicating loss of 60 Da and one loss of 18 Da (*m/z* 567, 507 and 489

respectively; Fig. 3d) are also present in the spectrum of peak **Ib** (as also seen for anhydroBHT; Fig. 3b) as well as the ion indicative of neutral loss of 192 (*m/z* 435; Fig. 3d). We conclude, therefore, that this compound is related to anhydroBHT but has an additional methylation, possibly in the side chain. The D/E+side-chain fragment in the EI mass spectrum would therefore be an ion of *m/z* 405. Two peaks are observed in the EI *m/z* 405 mass chromatogram (Fig. 1b); one, (peak **Ib**) eluting directly after the main anhydroBHT isomer (**Ia**) and a 2nd peak eluting later (peak **IIIb**, Fig. 1b). The EI mass spectrum of peak **Ib** (Fig. 3c) is consistent with these interpretations, as it includes the ions indicative of a regular hopanoid not methylated on the A/B rings (*m/z* 191) or indeed any part of the ring system (*m/z* 369) as also seen for regular anhydroBHT, but also the expected M^+ and $[M-15]^+$ ions of *m/z* 626 and 611, respectively.

The second peak in the *m/z* 405 mass chromatogram (**IIIb**; Fig. 1b) was more difficult to characterise by EI mass spectrometry as it co-eluted with a number of other known compounds including BHT (peak **Ic**, Fig. 1b) and multiple isomers of 32,35-anhydrobacteriohopanepentol (anhydroPentol, **Id**; Fig 1b; Talbot et al., 2005). The retention time of the later eluting *m/z* 405 peak relative to peak **Ib** is suggestive of an additional methylation at the C-3 position (e.g. Farrimond et al., 2004), supported by the presence of the m/z 205 and 383 ions in the EI mass spectrum (Fig. 3e). This peak (**IIIb**) could also be observed in the APCI data as a peak in the *m/z* 641 (= $[M+H]^+$) mass chromatogram (Fig. 1a). The assignment of an A/B ring methylation is indicated by the ion *m/z* 205 in the MS^2 spectrum (Fig. 3f) and the neutral loss of 206 Da after loss of 2 acetylated hydroxyls to give *m/z* 315. The relative retention time of peaks **Ib** and **IIIb** by RP-HPLC (Fig. 1a) also agrees with previously reported separations between non-methylated and C-3 methylated homologues via RP-HPLC (regular C-2 methylated structure would elute between **Ib** and **IIIb**; e.g. Talbot et al., 2003b). Therefore peaks **Ib** and **IIIb** are proposed as a pair of novel compounds related to anhydroBHT but with an additional methylation in the side chain and differing from each other by the presence of a methyl group at C-3 in the latter compound.

In a few samples which contained peak **Ib** ("side chain-methylated" anhydroBHT; see Table 1), a small shoulder was observed on the leading edge of this peak (peak **IIa**, Fig. 1a). For this shoulder, under APCI conditions, the MS^2 spectrum of m/z 627 did contain a small *m/z* 205 ion and it is therefore proposed to be the C-2 methylated homologue of anhydroBHT (**IIa**; e.g. Bednarczyk et al., 2005). However, this shoulder could not be readily distinguished from the main, non-methylated compound and therefore measurements of peak **Ib** incorporate a minor contribution for peak **IIa** which is estimated to account for less than 10% of the main peak where present.

3.1.3 Novel N-containing BHPs

In addition to the "regular" *N*-containing biohopanoids (Figs. 2 and 4a-c) other N-containing compounds were observed throughout the core including the recently described "anhydroaminotriol" (**Ii**, Figs. 2 and 4d; see Eickhoff et al., 2014). Identification of anhydroaminotriol can be difficult by GCMS as the intensity of response of nitrogen containing compounds via EI MS is much weaker than that of equivalent N-free compounds (e.g. Eickhoff et al., 2014). Furthermore, under RP-HPLC-APCI-MS analysis, anhydroaminotriol-triacetate co-elutes with regular aminotriol (peaks **Ii** and **If** respectively, Fig. 2). In addition, the triacetate has a base peak ion of *m/z* 654 (= $[M+H]^+$) which is equivalent to the primary fragment ion of aminotriol under the same conditions (aminotriol *m/z* 654 = $[M+H\text{-}CH_3COOH]^+$; Fig. 4a; Talbot et al., 2003b,c). However, careful inspection of the APCI data can still yield clues to the presence of this compound. Firstly, in the absence of anhydroaminotriol, the intensity of the aminotriol base peak ion (MH^+ = *m/z* 714) relative to the *m/z* 654 ion (= $[MH\text{-}CH_3COOH]^+$) in the full mass spectrum (Scan 1; Section 2.3) with the conditions used is typically in the range 5:1. Therefore, when the observed ratio is closer to 1:1 or higher as observed in several of the Cobham samples (Table 1, column m/z 654/m/z 714), it is clear that the transformation product is present. This assignment is also supported by consideration of the MS^n spectra of *m/z* 714 and 654 respectively. It has

previously been shown that MS^3 fragmentation of the *m/z* 654 ion derived from MS^2 of *m/z* 714 (aminotriol) leads to further fragmentation with ions *m/z* 594 and 534 as the major products (Talbot et al., 2003c). However, in the presence of anhydroaminotriol, during direct MS^2 fragmentation of *m/z* 654, the major ion observed is still *m/z* 654 (at 35% collision energy; Eickhoff et al., 2014), with lower intensity ions resulting from losses of 60 Da (acetylated OH groups at C-33 and C-34; Fig. 4d). This is a result of the stability of the heterocylic N atom during ion-trap fragmentation. Anhydroaminotriol was present in most samples and was always the most abundant N-containing degradation product (Table 1). Adjustment of the anhydroaminotriol peak area for relative quantification is described in section 2.3.

We also identified 2 other compounds which we tentatively propose to be novel *N*-containing BHP transformation products. The MS^2 spectrum (Fig. 4e) of peak **Ik** from the APCI *m/z* 728 mass chromatogram (Fig. 2) indicates a N-containing compound (on the basis of the even numbered base peak ion) with a minor ion of *m/z* 191 (intensity typical of N-containing BHPs; e.g. Fig. 4c). The base peak ion is equivalent to that of regular A/B ring methylated-aminotriol (e.g. Talbot et al., 2008), however, if that were the case the peak should elute directly after aminotriol (peak **If**, Fig. 2; Talbot et al., 2003b; 2008). The peak in question actually elutes significantly earlier suggesting a more polar compound. Speculating therefore that the 14 Da difference could result from the incorporation of ketone oxygen into the molecule, it is reasonable to expect a loss of that oxygen atom as water (18 Da) under APCI conditions. The major fragment ion in the MS^2 spectrum is *m/z* 710 (base peak minus 18 Da; Fig. 4e) with 3 further losses of 60 Da (3 acetylated hydroxyls) and a minor ion at *m/z* 471 resulting from a final loss of an acetylated amine (see Fig. 4c for comparison of intensity of ion indicating loss of amine in aminopentol spectrum). It is therefore proposed that peak **Ik** (Fig. 2) is related to aminotriol and contains an amine, 3 hydroxyls and a ketone. Although the location of the ketone cannot be constrained other than excluding the A/B rings on the basis of the minor *m/z* 191 ion, there is one previous report of a highly functionalised BHP

containing a ketone oxygen at the C-32 position in the side chain. The composite structure 32-oxo-bateriohopanetriol glucosamine (**Io**) was reported from *Zymomonas mobilis*, an obligately ethanologenic species of alphaproteobacteria (Flesch and Rohmer, 1989). It is therefore proposed that the most likely location for the ketone is at C-31 i.e. 31-oxo-35-amino-bacteriohopane-32,33,34-triol (31-oxo-aminotriol; Fig. 4e).

There was no equivalent peak in the *m/z* 786 chromatogram to indicate a possible hexafunctionalised compound (i.e. "30-oxo-aminotetrol"), even in the samples with the highest level of aminopentol. However, a peak of *m/z* 670 would correspond to the anticipated base peak for an aminodiol with additional ketone functionality. Peak **Ij**, the only significant peak in the *m/z* 670 mass chromatogram (Fig. 2), was considered to be a likely target. Note this retention time is too early to indicate a regular A/B ring methylated compound and the retention time relative to aminotriol (**If**) is early, as seen for the proposed ketone containing 31-oxo-amino-triol and aminotetrol (peaks **Ik** and **Ig** respectively, Fig. 2). Interpretation of this spectrum was complicated, however, as in many cases the peak co-eluted with an ion of *m/z* 669 meaning that the APCI spectrum contains fragments from both parent ions. Fragment ions of *m/z* 652, 610 and 550 were observed and would correspond exactly to the expected losses of the ketone oxygen as water or 2 acetylated OH functionalities. In this compound (**Ij**) the intensity of the $[M+H-18]^+$ ion (*m/z* 652) was significantly lower than for the equivalent ion (*m/z* 710) in the MS^2 spectrum of the proposed 31-oxo-aminotriol (**Ik;** Fig. 4e) whilst in the less functionalised compound, loss of the first acetylated hydroxyl (m/z 619) appears to be a more favourable fragmentation. A minor ion at 491 indicates loss of the acetylated OH groups and amine, prior to loss of the ketone, however, the hopanoid-specific ions at *m/z* 191 and 163 could be products of fragmentation of the co-eluting *m/z* 669 ion (see below). Therefore the assignment of peak **Ij** (Figs. 2 and 4f) as a tetrafunctionalised amine and ketone-containing BHP i.e. 32-oxo-35-amino-bacteriohopane-33,34-diol remains tentative but is included in further discussions below.

438 3.1.4 Other novel BHPs not containing a nitrogen atom

439 As mentioned above, a peak was observed in the *m/z* 669 APCI mass chromatogram which,
440 in samples where co-elution with peak **Ij** (m/z 670) was least significant, produced an APCI
441 spectrum potentially indicating a polyfunctionalised BHP (Fig. 5a). Although a peak of *m/z*
442 669 would typically indicate an A/B ring methylated BHT (Talbot et al., 2003c) the early
443 retention time (i.e. earlier than BHT; **Ic,** Fig. 1a) indicates a more polar component.
444 Assuming the validity of the assignment of peak **Ik** (Figs. 2 and 4e) as a ketone-containing
445 pentafunctionalised aminoBHP, it is then reasonable to assume that the same should be
446 possible for BHPs which do not contain nitrogen i.e. structures related to BHT. A base peak
447 of *m/z* 669 and retention time earlier than that of BHT is therefore suggestive of a BHT-
448 ketone (*m/z* 669 = $[M+H-CH_3COOH]^+$). The APCI spectrum of peak **Ie** (Fig. 5a) shows three
449 losses of 60 Da (*m/z* 609, 549 and 489 respectively) assumed to be the normal losses in the
450 APCI spectrum of regular BHT (Talbot et al., 2003b,c). Although an ion of *m/z* 471 could be
451 observed (loss of ketone oxygen as water from m/z 489), this was weak; nonetheless, the
452 hopanoid nature of this peak is confirmed by the *m/z* 191, 163 and ions following neutral loss
453 of the A+B rings (m/z 477, 417, 357; Fig. 5a).
454
455 As this compound does not contain N, an equivalent peak was sought in the GCMS data.
456 The anticipated parent ion for this peracetylated compound would be *m/z* 728 under EI and,
457 assuming a side chain location for the ketone, a D/E+side chain fragment 14 Da higher than
458 that of BHT i.e. *m/z* 507 (relative to *m/z* 493, Fig 5b) is expected. A peak (*m/z* 507, **Ie**; Fig.
459 1b) was observed eluting after the main *m/z* 493 peak in the GCMS data (**Ic**; Fig. 1b). The EI
460 mass spectrum of peak **Ie** (Fig. 5b) contained the typical hopanoid fragments of *m/z* 191 and
461 369 excluding any further modification from the ring system. The predicted D/E-side chain
462 fragment of *m/z* 507 was observed, however, so were two additional ions of *m/z* 447 and
463 387, potentially 2 losses of 60 Da from the full D/E-side chain fragment which are not
464 typically observed in other EI spectra of functionalised BHPs (e.g. Fig. 3a) but may be due to
465 the presence of the ketone. As the ring system ions restrict the location of the additional 14

Da to the side chain and in both the APCI and EI data, the relative retention time (compared to regular BHT; peak **Ic**) indicates a more polar structure than that resulting from a simple methylation, we conclude that there is a ketone present in this structure, located somewhere in the side chain, most likely at C-31 i.e. 31-oxo-BHT (**Ie**).

The tetrafunctionalised ketone equivalent (i.e. BHT with one OH replaced by ketone) would theoretically have an APCI base peak ion of *m/z* 611 ($[MH\text{-}CH3COOH]^+$). Two peaks were observed in this mass chromatogram in many samples, however, they also co-elute exactly with peaks in the *m/z* 671 chromatogram (Fig. 1a). The latter ion is also previously reported as the base peak ion for anhydropentol (**Id**) which has a major fragment ion of *m/z* 611 (Fig. 5c; Talbot et al., 2005) so the tetrafunctionalised ketone could not be confirmed by APCI-MS^n. Under EI conditions, the D/E-side chain fragment of this proposed ketone would be *m/z* 449, identical to that of anhydropentol (Figs 1b; see Talbot et al., 2005) and therefore could not be confirmed due to co-elution with multiple BHPs (Fig. 5d) although the anticipated $[M\text{-}15]^+$ ion was present in low abundance (Fig. 5d). This compound is therefore excluded from the following discussion of relative abundance of the various known biohopanoids and novel BHPs including functionalised transformation products.

To summarise, a range of polyfunctionalised biohopanoids were identified including strong evidence for methanotroph-derived BHPs (aminotetrol and aminopentol in particular but also aminotriol) as well as a recently identified N-containing diagenetic product (anhydroaminotriol) and a number of putative novel diagenetic products including structures with an unusual side-chain methylation. A diverse range of ketone containing products, termed “oxo” BHPs on the basis of previous studies (Flesch and Rohmer, 1989), both with and without a nitrogen atom in the structure, are tentatively assigned here for the first time.

3.2 BHP variations in the Cobham Lignite sequence

493 The compounds BHT (**Ic**), aminotriol (**If**) and aminotetrol (**Ig**) had very similar distributions in
494 the sequence when converted to % total BHPs, with the highest relative abundance in the
495 middle clay unit between the laminated and blocky lignite. However, these compounds were
496 also relatively abundant in the uppermost laminated lignite and the lowest blocky lignite
497 samples. Both of these lignite samples, to either side of the middle clay layer, also contained
498 clay laminae not seen in any other lignite samples (Table 1). The combined total abundance
499 of all biological BHPs relative to putative geo-BHPs shows two major and one minor peak
500 (Fig. 6c). The first major peak begins in the uppermost laminated lignite and spans the
501 middle clay layer reaching 100% biohopanoids at 65.3 cm (within the middle clay layer;
502 Table 1). The second maximum of 76% occurs near the top of the Blocky Lignite at 118.65
503 cm (Table 1; note the blocky lignite continues above the section investigated here; Collinson
504 et al., 2007; Steart et al., 2007). All biohopanoids show elevated levels in the samples from
505 115.65 and 118.65 cm except aminopentol which was only present in the lower of the two
506 samples where it is at its highest relative abundance throughout the entire sequence (4%;
507 Figs. 2 and 6, Table 1). The minor peak occurs in the single sand/mud unit sample
508 underlying the Cobham Lignite sequence (Fig. 6c). At the onset of the CIE (Fig. 6a,b; 54-56
509 cm) relative abundances of BHT, aminotriol and aminopentol fluctuate markedly (Fig. 6d, e
510 and g) whilst aminotetrol is consistently lower than in samples immediately pre and post this
511 interval (Fig. 6f). Aminopentol (**Ih**), however, was not present in the middle clay whilst both
512 BHT and Aminotetrol had higher relative abundance (to total biohopanoids) in the middle
513 clay layer and the adjacent lignite with clay samples (Table 1; Figs. 6d and 6f respectively).
514
515 The most abundant geo-BHP in the majority of samples was anhydroBHT (**Ia**) accounting for
516 up to 100% of all hopanoids (one sample; Fig. 7d, Table 1). Most of the geohopanoids
517 followed a similar trend to anhydroBHT with high abundances relative to biohopanoids in
518 lignites both above and below the middle clay layer (Table 1). This was particularly
519 noticeable for the N-containing compounds in the laminated lignite, especially in samples
520 leading up to and within the onset of the CIE just below the middle clay layer.

Anhydroaminotriol (**Ii**) reached a maximum of 45.8 % of the total BHPs and 50% of the total geohopanoids (40.65 cm, Table 1; Fig. 7g). The novel "side-chain methylated" anhydroBHTs (**Ib** and **IIIb**; Fig. 7e) and the proposed oxo-BHPs (**Ie**, **Ii**, **Ij**; Fig. 7f, h-, Table 1) all had similar profiles through the sequence with peaks coinciding with the onset of the CIE and at the end or just after deposition of the middle clay layer.

4. Discussion

4.1 Origin of BHPs in the Cobham Lignite sequence

4.1.1 Modern, Recent or Ancient deposition?

Palaeoenvironmental interpretation of BHPs in the Cobham Lignite is contingent on these BHPs being formed in the ancient environment rather than being derived from bacteria living in the shallow subsurface at any point post deposition to date. Previous workers have shown that bacteria do live in subsurface environments including in marine sediments (e.g. Parkes et al., 2000; Kallmeyer et al., 2012), lignites and coalbeds (e.g. Kotelnikova, 2002; Pokorný et al., 2005). Inagaki et al. (2015) found unexpectedly high levels of microbial cells in lignite layers buried ~ 2 km below the ocean floor and microbial community analysis revealed populations similar to those found in forest soils. Aerobic organisms can receive low levels of oxygen via meteoric water in the subsurface environment (e.g. Kotelnikova, 2002) and specific aerobic methanotrophic activity was recently identified in Carboniferous coals where organisms affiliated with the Type I genera *Methylomicrobium* and *Methylocaldum* and the Type II genera *Methylosinus* and *Methylocystis* were identified via 16S rRNA targeted gene sequencing after enrichment (Stepniewska et al., 2013). All of these genera have been shown to produce hopanoids (Cvejic et al., 2000; Talbot et al., 2001 and references therein; Banta et al., 2015), although both of the Type I genera identified are known to make both non-methylated and C-3 methylated biohopanoids (with a C-35 amine functionality), so are unlikely to be significant sources in the Cobham Lignite sequence which did not contain any

548 C-3 biohopanoids or hopanes (Pancost et al., 2007) and only one minor geohopanoid BHP
549 (side chain-methylated-3-methylanhydroBHT, **IIIb**). In light of these findings it is difficult to
550 preclude a modern origin for some of the biohopanoid BHPs at Cobham.
551
552 A modern origin for the Cobham Lignite BHPs, however, is considered unlikely for several
553 reasons. Firstly, many aspects of the BHP distribution are consistent with an aerobic source
554 which may be more recent but would also be consistent with formation in an ancient mire
555 with abundant methanotrophs. Previously, carbon isotopic analysis of the hopanes in the
556 same sample extracts (Fig. 6b, 7b; Pancost et al., 2007) supported a methanotrophic
557 source. For example, within the upper part of the laminated lignite at the onset of the CIE,
558 the $\delta^{13}C$ values of the C_{29}- and C_{31} 17β(*H*),21β(*H*) hopanes decrease (to values as low as -
559 76‰ and -42‰, respectively), indicating the consumption of isotopically light methane
560 (Pancost et al., 2007). This change in isotope values occurred within the laminated lignite
561 (section 2.1; Fig. 6), but below the transitional zone to the middle clay where thin clay
562 laminae start to appear in the lignite. Therefore the isotopic changes are not linked to
563 changes in depositional environment (as far as those are expressed by changes in lithology)
564 apparently precluding a preservation artefact (Pancost et al., 2007). Within the BHP
565 assemblage, the co-occurrence of aminotriol (**If**) and aminotetrol (**Ig**) and with a **If/Ig** ratio
566 less than 20 (as observed in all samples here, except that at 11.95 cm; Table 1) appears to
567 be indicative of an aerobic methanotroph source. Indeed the value is more frequently below
568 10, whereas the lowest reported values for the only other known source of aminotetrol,
569 anaerobic sulfate reducing bacteria of the genus *Desulfovibrio* (which are unlikely to occur in
570 a freshwater environment) is over 20 and can be as high as 100 (Blumenberg et al., 2006,
571 2009, 2012; See also review in Talbot et al., 2014). An aerobic methanotroph source is also
572 supported by the occurrence of aminopentol (**Ih**) in 13 samples covering all parts of the
573 sequence, except the middle clay layer (and the lignite samples directly above and below the
574 clay) where aminotetrol dominated (Figs. 6f and 8, Table 1).
575

Secondly, the strong increase in the relative proportion of biohopanoids in the middle clay layer and samples directly above and below containing clay laminae (Fig. 6c) is directly related to lithology. Low permeability of the clay layer compared to lignite would likely result in a much smaller “recent” population whilst the organic rich, more permeable lignite might be expected to host a larger “recent” population (cf. Inagaki et al., 2015). As the relative abundance of biohopanoid BHPs is in fact significantly lower in the lignite sections (Fig. 6c, 7c), this supports a sub-recent source for (some of) the BHPs with potentially better preservation of ancient BHPs in the fine grained material.

Thirdly, although modern bacteria could be affected by variations in lithology and organic matter content, they would not be expected to vary across the CIE onset, which occurs within the laminated lignite lithology below the transition zone to the clay layer (Figs. 6 and 7) where a distinct geohopanoid BHP signature with enhanced relative abundance of N-containing transformation products is observed (54.4 to 56.6 cm; Fig. 7h). Following the same argument made for the hopane isotope signature, that the lack of a change in lithology at this depth (54.4 to 56.6 cm) precludes a preservation artefact (Pancost et al., 2007), then an alternative explanation is required to explain the relative increase in ketone-containing compounds (Fig. 7f,h). As the pathway for production of the proposed ketone-containing compounds is currently unknown, they may represent either a specific transformation pathway, or could be derived from as yet unknown biological sources. The only previous report of a ketone containing biohopanoid was from the obligately ethanologenic bacterium *Zymomonas mobilis* (alphaproteobacteria; Flesch and Rohmer, 1989). This organism was cultured under microaerophilic conditions and the authors proposed that the compound 32-oxo-BHT glucosamine (**Io**) could be either a precursor or catabolite of BHT (Flesch and Rohmer, 1989). Gibson (2011) also tentatively identified ketone-containing polyfunctionalised hopanoids (without nitrogen) in geothermal sinters that were precipitating under microaerophilic conditions. We therefore tentatively propose that the oxo-amineBHPs could represent production by methanotrophs under oxygen limited conditions.

Finally, no composite BHPs (structures containing a more complex moiety at the C-35 position such as an aminosugar; e.g. **Im, In**; Rohmer, 1993) were observed, even in the clay layer, although these compounds would be expected in any modern or Recent terrestrial setting (e.g. Cooke et al., 2008a; van Winden et al., 2012a,b; Spencer Jones et al., 2015) including marine sediments containing high terrestrial fluvial input (e.g. Handley et al., 2010; Wagner et al., 2014). Furthermore, adenosylhopane (**Ip**), and compounds related to this structure containing an alternative terminal moiety at C-35 with or without A-ring methylation (**I** or I**Iq**) (e.g. Cooke et al., 2008a; Rethemeyer et al., 2010), were also absent from the Cobham sequence, despite being nearly ubiquitous in terrestrial settings (see review in Spencer-Jones et al., 2015). This is not surprising, if the BHPs that are present are indeed of Eocene age, as adenosylhopane was found to be degraded more rapidly than all other functionalised BHPs, including aminoBHPs, in a study of sediments up to 1.2 Ma from the Congo deep-sea fan (ODP site 1075; Cook et al., 2008b; Handley et al., 2010). Adenosylhopane was also completely removed/transformed during an artificial maturation experiment on biomass of the purple non-sulfur bacterium *Rhodopseudomonas palustris,* whilst some BHT (**Ic**) and aminotriol (**If**) remained after exposure to elevated pressure and temperature (170°C, 120 MPa, 7 d; Eickhoff et al., 2014).

Collectively, this evidence suggests that at least some of the BHPs, and the oxo-compounds in particular (Fig. 7f,h), could reflect environmental conditions associated with the original deposition of the lignite. Nonetheless, a more recent source can neither be confirmed nor entirely excluded and we suggest that future work conduct BHP analyses in tandem with microbiological investigations (i.e. cell counts, enrichments) in an attempt to decouple ancient from modern living bacterial contributions. If, however, the biohopanoid BHPs in the Cobham lignite are indeed of the same age as the deposition of the lignite, this would represent the oldest example of suites of solvent extractable intact biohopanoids reported to date. Previously only BHT has been identified in TLE from Tanzanian sediments up 50 Ma

(van Dongen et al., 2006) and following chemical degradation of the Messel oil shale kerogen (Eocene, 50 Ma; Mycke et al., 1987). If contemporaneous with lignite deposition then this significantly extends the aminoBHP record back in time, by nearly 55 Ma, highlighting their potential utility in identifying the aerobic methane oxidation process in samples where other methods can be inconclusive.

4.1.2 Variability in methanotrophic sources

The occurrence of aminopentol (**Ih**), thought to be a marker for Type I methanotrophs in terrestrial settings (see review in Talbot et al., 2014), in 13 Cobham Lignite samples is consistent with a significant methanotroph input. In recent studies aminopentol accounted for only a very minor proportion of the full biohopanoid BHP complement in a range of European *Sphagnum* peat sections (<1%; van Winden et al., 2012a,b; Talbot and Pancost, unpublished data). In contrast, the highest abundance of aminopentol relative to total biohopanoid BHPs in the Cobham Lignite reaches ~20% (sample 115.65 cm; Fig. 6g) or 4% relative to total BHPs (Table 1), significantly higher than that observed in any *Sphagnum* sample or modern peat. Furthermore, the peak occurrence of aminopentol (115.65 cm, Fig. 6g) corresponds to a C_{29} hopane carbon isotope ratio of -53.2‰ which, although less than the maximum depletion during the onset of the CIE, is still significantly depleted relative to pre-CIE values in the lower Laminated lignite (range -40.5 to -31.0‰; Fig 6b). Also, 3 of the 5 samples at the onset of the CIE where C_{29} carbon isotope ratio reach values as low as -75.7‰ also contain relatively high levels of aminopentol (up to 10% of total biohopanoids, Fig. 6g). The sample at 70.3 cm, slightly above the clay layer also contains similar levels of aminopentol and again corresponds to strongly depleted signature for the C_{29} hopane of -61.77‰ (Fig. 6b). Clearly there is correspondence in the Cobham Lignite between aminopentol abundances (as proportions of total biohopanoids) and ^{13}C-depleted isotopic composition of the C_{29} hopane. Moreover, maxima in aminopentol proportions and minima in C_{29} hopane $\delta^{13}C$ values also correspond to maxima in abundances of nitrogen and ketone-containing degradation products (Fig. 7h).

660

661 Aminotetrol (**Ig**) is also likely derived from methanotrophs in this terrestrial setting. It has also
662 been found only at very low levels in *Sphagnum* peat (<2% of total BHPs) such that its
663 relative abundance in the Cobham Lignite, reaching a maximum of ~65% of total
664 biohopanoid BHPs (Fig. 6f, 4.65 cm; equivalent to 14.4% of total BHPs; Table 1) is
665 remarkable, likely reflecting intense methanotrophic activity. Intriguingly and in contrast to
666 aminopentol, aminotetrol proportions do not appear to track hopane $\delta^{13}C$ values; in part, that
667 could reflect changing methanotroph communities as discussed below.

668

669 Aminotriol (**If**) and BHT (**Ic**) are much more significant components in peat (van Winden et
670 al., 2012a,b; Talbot and Pancost, unpublished data) than aminopentol and aminotetrol. They
671 are present throughout the Cobham sequence likely indicating a combination of sources
672 including Type II methanotrophs and heterotrophs (e.g. van Winden et al., 2012a). Again,
673 variations in their proportions do not correspond to those of hopane $\delta^{13}C$ values, suggesting
674 that they either do not derive from methanotrophs or derive from a different group of
675 methanotrophs, exhibiting different behaviour.

676

677 The BHP composition of both the lower laminated lignite (deposited during the latest
678 Palaeocene) and upper blocky lignite (deposited during the PETM) are broadly similar (Fig.
679 8a,d), suggesting the microbiological community was similar during both periods of
680 deposition or during later colonisation. If the former, this is unexpected given the wetter
681 conditions and presumably greater methane cycling (as inferred from hopane $\delta^{13}C$ values) in
682 the upper section, although Sherry et al. (2016) showed that there was no significant
683 changes in the overall methanotrophic community distribution in sediment slurry incubations
684 under a range of methane concentrations. Nonetheless, the blocky lignite is associated with
685 generally higher proportions of aminopentol (Fig. 6g) and that does suggest that aspects of
686 the biohopanoids BHP distribution are recording environmental change.

687

688 The most significant change in biohopanoid BHPs, both in terms of their abundance relative
689 to total BHPs and their distribution, occurs in the clay layer (and lignite with clay; Fig. 8c,
690 Table 1). Biohopanoid BHPs represented the highest proportion of total BHPs in the clay
691 layer, up to 100% at 65.3 cm (Fig. 6c; Table 1), which we attribute to enhanced preservation
692 (see above, section 4.1.1). With respect to the biohopanoid BHP distribution, the most
693 striking feature in the clay layer is the absence of aminopentol (**Ih**), particularly given the
694 high abundances of both aminotriol (**If**) and aminotetrol (**Ig**; Figs. 6e and f, 8b, Table 1). This
695 could reflect a change in the depositional environment: the clay layer has been linked to
696 changes in local hydrology leading to increased run-off and even standing water as indicated
697 by the occurrence of S*alvinia* and *Azolla* (free floating water plants) at the base of the blocky
698 lignite directly above the clay, possibly facilitated by deposition of clay reducing drainage
699 (Collinson et al., 2003, 2013; Steart et al., 2007 and references therein). This could have
700 impacted bacterial or even methanotroph communities and associated BHP signatures.
701

702 The presence of aminotetrol and absence of aminopentol has been linked to Type II
703 methanotroph sources (e.g. Talbot et al., 2001; Birgel et al., 2011), although some Type I
704 methanotrophs also do not produce aminopentol (Talbot et al., 2001; Jahnke et al., 1995;
705 Coolen et al., 2008; Banta et al., 2015). Nonetheless, it is possible that the different
706 distributions in the clay layer reflect different environmental conditions and a methanotroph
707 community dominated by Type II organisms. These are traditionally believed to be common
708 in terrestrial settings (soils, peats e.g. Hanson and Hanson, 1996), although this is certainly
709 not always the case. For example, Gray et al. (2014) found that Type I methanotrophs
710 dominated over Type II signals in soil cores from 13 sites located along the southern and
711 northern margins of Kongsfjorden in Northwestern Spitsbergen. Overall, it remains unclear
712 what dictates the predominance of different types of methanotrophs, and therefore, it is
713 difficult to explain a change in assemblages in the Cobham Lignite.

4.2 Known and novel polyfunctionalised hopanoid transformation products in the Cobham Lignite sequence

4.2.1. AnhydroBHT and related structures

The most abundant degradation product, occurring in all but one sample (65.3 cm; Table 1) in the Cobham sequence was anhydroBHT (**Ia**). This is expected as the compound has been shown to be produced from BHT (**Ic**) and composite structures such as BHT cyclitol ether (**Im**) under a range of conditions (Schaeffer et al., 2008, 2010; Eickhoff et al., 2014). It has been reported in a wide range of samples as old as Jurassic in age (Bednarczyk et al., 2005) and was by far the most abundant BHP in a ~50 Ma marine sediment sample from Tanzania (van Dongen et al., 2006). Watson (2002), also showed a correlation between loss of BHT and increase in anhydroBHT in sediments from the Benguela upwelling system down to over 4 Ma, as did Blumenberg et al. (2013) in younger sediments from the Baltic Sea. Whilst it is yet to be conclusively demonstrated that adenosylhopane (**Ip**; or related compounds, **Iq**) could also be a precursor for this transformation product, a number of studies have speculated that it may be possible via reductive removal of the terminal adenine (Costantino et al., 2001; Cooke et al., 2008b; Eickhoff et al., 2014). The high abundance of anhydroBHT in these samples, therefore, likely indicates an amalgamated signature from a range of precursor biohopanoids.

By careful inspection of the APCI and EI data we have identified 2 novel structures related to anhydroBHT (**Ia**) but containing an unusual methylation in the side chain (Figs. 1 and 3). The location of the unusual side chain methylation could not be conclusively determined based on the available data and insufficient material is available to attempt isolation and NMR analysis. Previously, however, Simonin et al. (1994) identified biohopanoids with methylation at the C-31 position of the side chain of hopanoids from the acetic acid bacterium *Acetobacter europaeus* (Phylum Alphaproteobacteria, also known as *Gluconacetobacter europaeus* or *Komagataeibacter europaeus*). The side chain methylated compounds in that study were also methylated at the C-3 position as in compound **IIIb** reported here (Fig. 3).

742 More recently, Nytoft (2011) reported C-31 methylated hopanes, although not additionally
743 methylated at the C-3 position, in coals and crude oils sourced from a range of locations
744 worldwide and linked these compounds with oxic depositional environments. The possible
745 occurrence of C-3 methylation in one of these structures (**IIIb**), the only proposed C-3
746 methylated compound in the entire data set, does agree with the potential acetic acid
747 bacterium source (Simonin et al., 1994); therefore the tentative structures are illustrated with
748 the methylation at C-31 (**Ib** and **IIIb**; Fig. 3 and Appendix). An alternative known site for
749 methylation at C-12 as reported for a BHT in the sponge *Placortis simplex* (Costantino et al.,
750 2000) could be conclusively ruled out for structure **Ib** due to the presence of the m/z 369 ion
751 in the EI spectrum (Figs. 3c). No C-3 methylated precursor biohopanoids were observed in
752 the Cobham sequence; however, given the low relative intensity of peak **IIIb** (Fig. 1; Table
753 1), this is not surprising, especially when considering that reports of other C-3 methylated
754 biohopanoids in younger samples are scarce (e.g. Talbot et al., 2003a; Talbot and
755 Farrimond, 2007; Blumenberg et al., 2007; Gibson et al., 2008; Zhu et al., 2011).
756
757 We are not aware of prior reports of polyfunctionalised biohopanoids with this unusual side-
758 chain methylation in environmental samples. The relative retention time of **Ib** to anhydroBHT
759 (**Ia**; Fig. 1) indicates that it would elute in approximately the same position as the regular C-2
760 methylated homologue (**IIa**; Fig.1). However, in various settings an apparently methylated
761 BHT eluting at the expected C-2 methyl position (i.e. directly after BHT by RP-HPLC) has
762 been observed in sediment extracts but where the MS^2 spectrum contains a dominant m/z
763 191 and only a minor m/z 205 ion (if present at all; Talbot et al., unpublished data).
764
765 There was no evidence of C-2 methylated biohopanoid precursors in any of the samples,
766 and only trace levels of a C-2 methylated anhydroBHT (**IIa**) could be identified in a few
767 samples indicating that some C-2 methylated precursor was occasionally present. Absence
768 of C-2 methylated structures is relatively unusual for terrestrial settings, as they are
769 frequently found, for example, in soils (e.g. Cooke et al., 2008a; Xu et al., 2009; Rethemeyer

et al., 2010; Kim et al., 2011; Zhu et al., 2011), lake sediments (Talbot et al., 2003a; Talbot and Farrimond, 2007; Coolen et al., 2008) and tropical wetlands (Wagner et al., 2014; Spencer-Jones et al., 2015). As the co-eluting peak **Ib** was in all cases significantly more intense than the shoulder **IIa** (e.g. Fig. 1a), the compounds could not be individually integrated and are combined in Table 1. Furthermore, peak **IIa** could not be conclusively identified by GCMS analysis.

4.2.2 *N-containing transformation products.*

Crucially, this study has revealed the presence of both previously identified and novel transformation products of N-containing BHPs, providing new tools for examining methane cycling in ancient settings. These observations are consistent with recent experimental work. Eickhoff et al. (2014) reported the generation of a pair of novel *N*-containing transformation products during simulated diagenetic degradation of a culture of the purple non-sulfur bacterium *Rhodopseudomonas palustris*. These structures, tentatively identified as isomers of anhydroaminotriol (**Ii**; Fig. 4d), were major components of the products after artificial maturation. Their finding is significant as it represents the first polyfunctionalised N-containing hopanoid degradation product indicating a possible distinct transformation pathway for hopanoids containing a terminal amine (Eickhoff et al., 2014). The observation of the later eluting and therefore presumed $\beta\beta$ isomer here in the Cobham Lignite represents the first report of this compound from environmental samples. Moreover, other N-containing products are tentatively proposed here (oxo-aminotriol [**Ik**] and oxo-aminodiol [**Ij**]; Figs 2 and 4, Table 1). Anhydroaminotriol was by far the most abundant compound of this type during the onset of the CIE (Fig. 8c; Table 1), although its peak occurrence was in the sample from 40.65 cm suggesting that nitrogen containing precursors were particularly abundant at the time of deposition of this sample. However, bulk and compound specific isotope values do not indicate an enhancement in methane cycling at this point (Fig. 7; Pancost et al., 2007) and therefore suggest heterotrophic sources for the precursor aminotriol.

5. Conclusions

This study presents the first identification of polyfunctionalised bio- and geohopanoids in the well preserved, immature Cobham Lignite sequence from within part of the PETM interval (~56 Ma) and below. Up to four different biohopanoids including BHT, aminotriol, aminotetrol and aminopentol were observed in samples throughout the sequence. Although the age of the BHPs cannot be constrained at this time, several lines of evidence point to a sub-Recent, predominantly methanotrophic source for the BHPs. These include prior reports of isotopically light hopanes (up to -74‰) indicative of enhanced methanotrophy at the onset of the negative CIE, the absence of the composite biohopanoids or adenosylhopane and related structures, and peaks in novel, potentially ketone containing, geohopanoid BHP transformation products corresponding to the onset of the CIE.

The comparable averaged BHP distribution in the lower laminated lignite (deposited during the latest Paleocene) and the blocky lignite (deposited during the PETM) suggest similar dominant members of the microbiological community were active during both periods This is unexpected given the wetter conditions and the presence of generally more ^{13}C-depleted hopanes in the blocky lignite although there are subtle differences in the intermittent occurrence of aminopentol which corresponds with depleted C_{29} hopane $\delta^{13}C$ values.

Further experimental work (e.g. quantitative BHP analysis; laboratory studies of the impact of different environmental conditions [temperature, methane concentration etc.] on BHP distributions) and study of other lignites including cell counts, formed under both changing and constant climatic conditions, is needed to interpret the palaeoenvironmental implications of the methanotroph communities and their varied biomarkers.

822 ACKNOWLEDGEMENTS

823

824 We thank Alfred McAlpine plc, AMEC and Channel Tunnel Rail Link for access to the
825 Cobham Lignite sequence, and S. Rose for making arrangements; J. Hooker, J. Skipper and
826 S. Tracey for help with sample collection and field discussions. We thank J. Hooker for his
827 contributions to the understanding of the stratigraphy of the site. We acknowledge funding
828 support for this research from the Leverhulme Trust (Grant number F/07/537/0) and the
829 Natural Environment Research Council [Grant numbers NE/J008656/1] [NE/J008591/1]. This
830 project was also partially funded by a Starting Grant (No. 258734) awarded to HMT for
831 project AMOPROX from the European Research Council (ERC) and we also thank the
832 Natural Environment Research Council (NERC) for funding JB (Grant number
833 NE/I027967/1). We also thank the Science Research Investment Fund (SRIF) from HEFCE
834 for funding the purchase of the ThermoFinnigan LCQ ion trap mass spectrometer
835 (Newcastle) and Paul Donohoe, Kate Osborne, Luke Handley, Frances Sidgwick and David
836 Steart for technical assistance. Finally, we thank the associate editor and reviewers Martin
837 Blumenberg and Alex Sessions for their critical reviews which helped to significantly improve
838 the manuscript.

839

840 **References**

841 Banta, A., Wei, J.H., Welander, P.V., 2015. A distinct pathway for tetrahymanol synthesis in
842 bacteria. Proceedings of the National Academy of Science of the USA 112, 13478-13483.
843 Bednarczyk, A., Hernandez, T.C., Schaeffer, P., Adam, P., Talbot, H.M., Farrimond, P.,
844 Riboulleau, A., Largeau, C., Derenne, S., Rohmer, M., Albrecht, P., 2005. 32,35-
845 Anhydrobacteriohopanetetrol: An unusual bacteriohopanepolyol widespread in recent and
846 past environments. Organic Geochemistry 36, 673–677.
847 Berndmeyer, C., Thiel, V., Schmale, O., Blumenberg, M., 2013. Biomarkers for aerobic
848 methanotrophy in the water column of the stratified Gotland Deep (Baltic Sea). Organic
849 Geochemistry 55, 103-111.
850 Birgel, D., Feng, D., Roberts, H.H., Peckmann, J., 2011. Changing redox conditions at cold
851 seeps as revealed by authigenic carbonates from Alaminos Canyon, northern Gulf of
852 Mexico. Chemical Geology 285, 82–96.
853 Blumenberg, M., Krüger, M., Nauhaus, K., Talbot, H.M., Oppermann, B.I., Seifert, R., Pape,
854 T., Michaelis, W., 2006. Biosynthesis of hopanoids by sulfate-reducing bacteria (genus
855 *Desulfovibrio*). Environmental Microbiology 8, 1220–1227.
856 Blumenberg, M., Seifert, R., Michaelis, W., 2007. Aerobic methanotrophy in the oxic–anoxic
857 transition zone of the Black Sea water column. Organic Geochemistry 38, 84–91.
858 Blumenberg, M., Oppermann, B.I., Guyoneaud, R., Michaelis, W., 2009. Hopanoid
859 production by *Desulfovibrio bastinii* isolated from oilfield formation water. FEMS
860 Microbiology Letters 293, 73–78.
861 Blumenberg, M., Mollenhauer, G., Zabel, M., Reimer, A., Thiel, V., 2010. Decoupling of bio
862 and geohopanoids in sediments of the Benguela Upwelling System (BUS). Organic
863 Geochemistry 41, 1119–1129.
864 Blumenberg, M., Hoppert, M., Krüger, M., Dreier, A., Thiel, V., 2012. Novel findings on
865 hopanoid occurrences among sulfate reducing bacteria: is there a direct link to nitrogen
866 fixation? Organic Geochemistry 49, 1–5.

867 Blumenberg, M., Berndmeyer, C., Moros, M., Muschalla, M., Schmale, O., Thiel, V., 2013.
868 Bacteriohopanepolyols record stratification, nitrogen fixation and other biogeochemical
869 perturbations in Holocene sediments of the Central Baltic Sea. Biogeosciences 10, 2725-
870 2735.
871 Bodlenner, A., Liu, W.H., Hirsch, G., Schaeffer, P., Blumenberg, M., Lendt, R., Tritsch, D.,
872 Michaelis, W., Rohmer, M., 2015. C35 Hopanoid Side Chain Biosynthesis: Reduction of
873 Ribosylhopane into Bacteriohopanetetrol by a Cell-Free System from *Methylobacterium*
874 *organophilum*. ChemBioChem 16, 1764-1770.
875 Bradley, A.S., Pearson, A., Saenz, J.P., Marx, C.J., 2010. Adenosylhopane: The first
876 intermediate in hopanoid side chain biosynthesis. Organic Geochemistry 41, 1075-1081.
877 Burhan, R.Y.P., Trendel, J.M., Adam, P., Wehrung, P., Albrecht, P., Nissenbaum, A. 2002.
878 Fossil bacterial ecosystem at methane seeps: origin of organic matter from Be'eri sulphur
879 deposit, Israel. Geochimica et Cosmochimica Acta 66, 4085–4101.
880 Collinson, M.E., Hooker, J.J., Gröcke, D.R., 2003. Cobham Lignite Bed and
881 penecontemporaneous macrofloras of southern England: A record of vegetation and fire
882 across the Paleocene-Eocene Thermal Maximum. Geological Society of America Special
883 Papers 369, 333-349.
884 Collinson, M.E., Steart, D.C., Scott, A.C., Glasspool, I.J., Hooker, J.J., 2007. Episodic fire,
885 runoff and deposition at the Palaeocene-Eocene boundary. Journal of the Geological
886 Society, London 164, 87-97.
887 Collinson, M.E., Steart, D.C., Harrington, G.J., Hooker, J.J., Scott, A.C., Allen, L.O.,
888 Glasspool, I.J., Gibbons, S.J., 2009. Palynological evidence of vegetation dynamics in
889 response to palaeoenvironmental change across the onset of the Paleocene-Eocene
890 Thermal maximum at Cobham, Southern England. Grana 48, 38-66.
891 Collinson, M.E., Smith, S.Y., van Konijnenburg-van Cittert, J.H.A., Batten, D.J., van der
892 Burgh, J., Barke, J., Marone, F., 2013. New observations and synthesis of Paleogene
893 heterosporous water ferns. International Journal of Plant Sciences 174, 350-363.

894 Collister, J.W., Summons, R.E., Lichtfouse, E., Hayes, J.M., 1992. An isotopic
895 biogeochemical study of the Green River oil shale. Organic Geochemistry 19, 265–276.
896 Cooke, M.P., Talbot, H.M., Farrimond, P., 2008a. Bacterial populations recorded in
897 bacteriohopanepolyol distributions in soils from Northern England. Organic Geochemistry
898 39, 1347–1358.
899 Cooke, M.P., Talbot, H.M., Wagner, T., 2008b. Tracking soil organic carbon transport to
900 continental margin sediments using soil-specific hopanoid biomarkers: a case study from
901 the Congo fan (ODP site 1075). Organic Geochemistry 39, 965–971.
902 Coolen, M.J.L., Talbot, H.M., Abbas, B.A., Ward, C., Schouten, S., Volkman, J.K., Sinninghe
903 Damsté, J.S., 2008. Sources for sedimentary bacteriohopanepolyols as revealed by 16S
904 rDNA stratigraphy. Environmental Microbiology 10, 1783-1803.
905 Costantino, V., Fattorusso, E., Imperatore, C., Mangoni, A., 2000. The First 12-
906 Methylhopanoid: 12-Methylbacteriohopanetetrol from the Marine Sponge *Plakortis*
907 *simplex.* Tetrahedron 56, 3781-3784.
908 Costantino, V., Fattorusso, E., Imperatore, C., Mangoni, A., 2001. A biosynthetically
909 significant new bacteriohopanoid present in large amounts in the Caribbean sponge
910 *Plakortis simplex*. Tetrahedron 57, 4045–4048.
911 Cvejic, J.H., Bodrossy, L., Kovacs, K.L., Rohmer, M., 2000. Bacterial triterpenoids of the
912 hopane series from the methanotrophic bacteria *Methylocaldum* spp.: phylogenetic
913 implications and first evidence for an unsaturated aminobacteriohopanepolyol. FEMS
914 Microbiology Letters 182, 361–365.
915 Eickhoff, M., Birgel, D., Talbot, H.M., Peckmann, J., Kappler, A., 2014. Early diagenetic
916 degradation products of bacteriohopanepolyols produced by *Rhodopseudomonas*
917 *palustris* strain TIE-1. Organic Geochemistry 68, 31–38.
918 Farrimond, P., Talbot, H.M., Watson, D.F., Schulz, L.K., Wilhelms, A., 2004.
919 Methylhopanoids: Molecular indicators of ancient bacteria and a petroleum correlation
920 tool. Geochimica et Cosmochimica Acta 68, 3873-3882.

921 Flesch, G., Rohmer, M., 1989. Prokaryotic triterpenoids. A novel hopanoid from the ethanol-
922 producing bacterium *Zymomonas mobilis*. Biochemical Journal 262, 673-675.
923 Gibson, R.A., 2011. The distribution of bacteriohopanepolyols in terrestrial geothermal
924 ecosystems. PhD Thesis, Newcastle University, UK.
925 https://theses.ncl.ac.uk/dspace/bitstream/10443/1104/1/Gibson11.pdf
926 Gibson R.A., Kaur, P., Pancost, R.D., Mountain, B., Talbot, H.M., 2008.
927 Bacteriohopanepolyol signatures of cyanobacterial and methanotrophic bacterial
928 populations recorded in a geothermal vent sinter. Organic Geochemistry 39, 1020-1023.
929 Gibson, R.A., Sherry, A., Kaur, G., Pancost, R.D., Talbot, H.M., 2014.
930 Bacteriohopanepolyols preserved in silica sinters from Champagne Pool (New Zealand)
931 record the environmental history of the vent. Organic Geochemistry 69, 61–69.
932 Gray, N.D., McCann, C.M., Christgen, B., Ahammad, S.Z., Roberts, J.A., Graham, D.W.,
933 2014. Soil geochemistry confines microbial abundances across an Arctic landscape;
934 Implications for net carbon exchange with the atmosphere. Biogeochemistry 120, 307-
935 317.
936 Handley, L., Talbot, H.M., Cooke, M.P., Anderson, K.E., Wagner, T., 2010.
937 Bacteriohopanepolyols as tracers for continental and marine organic matter supply and
938 phases of enhanced nitrogen cycling on the late Quaternary Congo deep sea fan.
939 Organic Geochemistry 41, 910–914.
940 Hanson, R.H., Hanson, T.E., 1996. Methanotrophic bacteria. Microbiological Reviews 439–
941 471.
942 Inagaki, F., Hinrichs, K.-U., Kubo, Y., Bowles, M.W., Heuer, V.B., Hong, W.-L., Hoshino, T.,
943 Ijiri, A., Imachi, H., Ito, M., Kaneko, M., Lever, M.A., Lin, Y.-S., Methé, B.A., Morita, S.,
944 Morono, Y., Tanikawa, W., Bihan, M., Bowden, S.A., Elvert, M., Glombitza, C., Gross, D.,
945 Harrington, G.J., Hori, T., Li, K., Limmer, D., Liu, C.-H., Murayama, M., Ohkouchi, N.,
946 Ono, S., Park, Y.-S., Phillips, S.C., Prieto-Mollar, X., Purkey, M., Riedinger, N., Sanada,
947 Y., Sauvage, J., Snyder, G., Susilawati, R., Takano, Y., Tasumi, E., Terada, T., Tomaru,

948 H., Trembath-Reichert, E., Wang, D.T., Yamada, Y., 2015. Exploring deep microbial life in
949 coal-bearing sediment down to ~2.5 km below the ocean floor. Science 349, 420-424.
950 Jahnke, L.L., Summons, R.E., Dowling, L.M., Zahiralis, A.D., 1995. Identification of
951 methanotrophic lipid biomarkers in cold-seep mussel gills: chemical and isotopic analysis.
952 Applied and Environmental Microbiology 61, 576–582.
953 Jahnke, L.L., Summons, R.E., Hope, J.M., Des Marais, D.J., 1999. Carbon isotopic
954 fractionation in lipids from methanotrophic bacteria II: the effects of physiology and
955 environmental parameters on the biosynthesis and isotopic signatures of biomarkers.
956 Geochimica et Cosmochimica Acta 63, 79–93.
957 Kallmeyer, J., Pockalny, R., Adhikari, R.R., Smith, D.C., D'Hondt, S., 2012. Global
958 distribution of microbial abundance and biomass in subseafloor sediment. Proceedings of
959 the National Academy of Sciences 109, 16213-16216.
960 Kannenberg, E.L., Poralla, K., 1999. Hopanoid biosynthesis and function.
961 Naturwissenschaften 86, 168–176.
962 Kim, J.-J., Talbot, H.M., Zarzycka, B., Bauersach, T., Wagner, T., 2011. Occurrence and
963 abundance of soil-specific bacterial membrane lipid markers in the Têt watershed
964 (Southern France): soil-specific BHPs and branched GDGTs. Geochemistry, Geophysics,
965 Geosystems 12, number 2. doi:10.1029/2010GC003364
966 Kotelnikova, S., 2002. Microbial production and oxidation of methane in deep subsurface.
967 Earth-Science Reviews 58, 367 – 395.
968 Kulkarni, G., Wu, C.-H., Newman, D.K., 2013. The general stress response factor EcfG
969 regulates expression of the C-2 hopanoid methylase *HpnP* in *Rhodopseudomonas*
970 *palustris*TIE-1. Journal of Bacteriology 195, 2490-2498.
971 Liu, W., Sakr, E., Schaeffer, P., Talbot, H.M., Kannenberg, E., Donisi, J., Poralla, K.,
972 Takano, E., Rohmer, M., 2014. Ribosylhopane, a novel bacterial hopanoid, as precursor
973 of C35 bacteriohopanepolyols in *Streptomyces coelicolor* A3(2). ChemBiochem. 15,
974 2156-2161.

McInerney, F.A., Wing. S.L., 2011. The Paleocene-Eocene Thermal Maximum: A Perturbation of Carbon Cycle, Climate, and Biosphere with Implications for the Future. Annual Review of Earth and Planetary Sciences 39, 489–516.

Mycke, B., Narjes, F., Michaelis, W., 1987. Bacteriohopanetetrol from chemical degradation of an oil shale kerogen. Nature 326, 179 – 181.

Neunlist, S., Rohmer, M., 1985. Novel hopanoids from the methylotrophic bacteria *Methylococcus capsulatus* and *Methylomonas methanica* - (22S)-35-Aminobacteriohopane-30,31,32,33,34-pentol and (22S)-35-amino-3-β-methylbacteriohopane-30,31,32,33,34-pentol. Biochemical Journal 231, 635-639.

Nytoft, H.P., 2011. Novel side chain methylated and hexacyclic hopanes: Identification by synthesis, distribution in a worldwide set of coals and crude oils and use as markers for oxic depositional environments. Organic Geochemistry 42, 520-539.

Ourisson, G., Albrecht, P., 1992. Hopanoids. 1. Geohopanoids: The most abundant natural products on Earth? Accounts of Chemical Research 25, 398–402.

Ourisson, G., Rohmer, M., Poralla, K., 1987. Prokaryotic hopanoids and other polyterpenoid sterol surrogates. Annual Review of Microbiology. 41, 301–333.

Pancost, R.D., Steart, D.S., Handley, L., Collinson, M.E., Hooker, J.J., Scott, A.C., Grassineau, N.V., Glasspool, I.J., 2007. Increased terrestrial methane cycling at the Palaeocene-Eocene thermal maximum. Nature 449, 332-335.

Parkes, R.J., Cragg, B.A., Wellsbury P., 2000. Recent studies on bacterial populations and processes in subseafloor sediments: A review. Hydrogeology Journal 8, 11–28.

Pearson, A., Page, S.R.F., Jorgenson, T.L., Fischer, W.W., Higgins, M.B., 2007. Novel hopanoid cyclases from the environment. Environmental Microbiology 9, 2175-2188.

Pearson, A., Leavitt, W.D., Sáenz, J.P., Summons, R.E., Tam, M.C.M., Close, H.G., 2009. Diversity of hopanoids and squalene-hopene cyclases across a tropical land-sea gradient. Environmental Microbiology 11, 1208-1223.

Pokorný, R., Olejníková, P., Balog, M., Zifčák, Hölker, U., Janssen, M., Bend, J., Höfer, M., Holienčin, R., Hudecová, D., Varečka, L., 2005. Characterization of microorganisms

1003 isolated from lignite excavated from the Záhorie coal mine (southwestern Slovakia).
1004 Research in Microbiology 156, 932–943.
1005 Rethemeyer, J., Schubotz, F., Talbot, H.M., Cooke, M.P., Hinrichs, K.-U., Mollenhauer, G.,
1006 2010. Distribution of polar membrane lipids in permafrost soils and sediments of a small
1007 high Arctic catchment. Organic Geochemistry 41, 1130–1145.
1008 Rohmer, M., 1993. The biosynthesis of triterpenoids of the hopane series in the Eubacteria:
1009 A mine of new enzyme reactions. Pure and Applied Chemistry 65, 1293-1298.
1010 Rohmer, M., Bouvier-Nave, P., Ourisson, G., 1984. Distribution of hopanoid triterpenes in
1011 prokaryotes. Journal of General Microbiology 130, 1137–1150.
1012 Sáenz, J.P., Sezgin, E., Schwille, P., Simons, K., 2012. Functional convergence of
1013 hopanoids and sterols in membrane ordering. Proceedings of the National Academy of
1014 Science 109, 14236-14240.
1015 Schaeffer, P., Schmitt, G., Adam, P., Rohmer, M., 2008. Acid-catalyzed formation of 32,35-
1016 anhydrobacteriohopanetetrol from bacteriohopanetetrol. Organic Geochemistry 39, 1479–
1017 1482.
1018 Schaeffer, P., Schmitt, G., Adam, P., Rohmer, M., 2010. Abiotic formation of 32,35-
1019 anhydrobacteriohopanetetrol: A geomimetic approach. Organic Geochemistry 41, 1005–
1020 1008.
1021 Sessions, A.L., Zhang, L., Welander, P.V., Doughty, D., Summons, R.E., Newman, D.K.,
1022 2013. Identification and quantification of polyfunctionalized hopanoids by high
1023 temperature gas chromatography–mass spectrometry. Organic Geochemistry 56, 120–
1024 130.
1025 Sherry, A., Osborne, K.A., Sidgwick, F., Gray, N.D., Talbot, H.M., 2016. A temperate river
1026 estuary is a sink for methanotrophs adapted to extremes of pH, temperature and salinity.
1027 Environmental Microbiology Reports 8, 122-131.

1028 Simonin, P., Tindall, B., Rohmer, M., 1994. Structure elucidation and biosynthesis of 31-
1029 methylhopanoids from *Acetobacter europaeus*. European Journal of Biochemistry 225,
1030 765-771.
1031 Spencer-Jones, C.L., 2016. Novel concepts derived from microbial biomarkers in the Congo
1032 System: Implications for continental methane cycling. PhD Thesis. Newcastle University,
1033 UK.
1034 Spencer-Jones, C.L., Wagner, T., Dinga, B.J., Schefuß, E., Mann, P.J., Poulsen, J.R.,
1035 Spencer, R.G.M., Wabakanghanzi, J.N., Talbot, H.M., 2015. Bacteriohopanepolyols in
1036 tropical soils and sediments from the Congo River catchment area. Organic
1037 Geochemistry doi: http://dx.doi.org/10.1016/j.orggeochem.2015.09.003
1038 Steart, D.C., Collinson, M.E., Scott, A.C., Glasspool, I.J., Hooker, J.J., 2007. The Cobham
1039 lignite bed: the palaeobotany of two petrographically contrasting lignites from either side
1040 of the Paleocene-Eocene carbon isotope excursion. Acta Palaeobotanica 47, 109-125.
1041 Stępniewska, Z., Pytlak, A., Kuźniar, A., 2013. Methanotroph activity in Carboniferous
1042 coalbed rocks. International Journal of Coal Geology 106, 1-10.
1043 Talbot, H.M., Farrimond, P., 2007. Bacterial populations recorded in diverse sedimentary
1044 biohopanoid distributions. Organic Geochemistry 38, 1212–1225.
1045 Talbot, H.M., Watson, D.F., Murrell, J.C., Carter, J.F., Farrimond, P., 2001. Analysis of intact
1046 bacteriohopanepolyols from methanotrophic bacteria by reversed phase high
1047 performance liquid chromatography - atmospheric pressure chemical ionisation - mass
1048 spectrometry. Journal of Chromatography A 921, 175-185.
1049 Talbot, H.M., Watson, D.F., Pearson, E.J., Farrimond, P., 2003a. Diverse biohopanoid
1050 compositions of non-marine sediments. Organic Geochemistry 34, 1353–1371.
1051 Talbot, H.M., Squier, A.H., Keely, B.J., Farrimond, P., 2003b. Atmospheric pressure
1052 chemical ionisation reversed-phase liquid chromatography/ion trap mass spectrometry of
1053 intact bacteriohopanepolyols. Rapid Communications in Mass Spectrometry 17, 728–737.
1054 Talbot, H.M., Summons, R.E., Jahnke, L.L., Farrimond, P., 2003c. Characteristic
1055 fragmentation of bacteriohopanepolyols during atmospheric pressure chemical ionisation

1056 liquid chromatography/ion trap mass spectrometry. Rapid Communications in Mass
1057 Spectrometry 17, 2788–2796.
1058 Talbot, H.M., Farrimond, P., Schaeffer, P., Pancost, R.D., 2005. Bacteriohopanepolyols in
1059 hydrothermal vent biogenic silicates. Organic Geochemistry 36, 663–672.
1060 Talbot, H.M., Rohmer, M., Farrimond, P., 2007a. Rapid structural elucidation of composite
1061 bacterial hopanoids by atmospheric pressure chemical ionisation liquid
1062 chromatography/ion trap mass spectrometry. Rapid Communications in Mass
1063 Spectrometry 21, 880-892.
1064 Talbot, H.M., Rohmer, M., Farrimond, P., 2007b. Structural characterisation of unsaturated
1065 bacterial hopanoids by atmospheric pressure chemical ionisation liquid
1066 chromatography/ion trap mass spectrometry. Rapid Communications in Mass
1067 Spectrometry 21, 1613-1622.
1068 Talbot, H.M., Summons, R.E., Jahnke, L.L., Cockell, C.S., Rohmer, M., Farrimond, P., 2008.
1069 Cyanobacterial bacteriohopanepolyol signatures from cultures and natural environmental
1070 settings. Organic Geochemistry 39, 232–263.
1071 Talbot, H.M., Handley, L., Spencer-Jones, C.L., Dinga, B.J., Schefuß E., Mann, P.J.,
1072 Poulsen, J.R., Spencer, R.G.M., Wabakanghanzi, J.N., Wagner, T., 2014. Variability in
1073 aerobic methane oxidation over the past 1.2 Myrs recorded in microbial biomarker
1074 signatures from Congo fan sediments. Geochimica et Cosmochimica Acta 133, 387-401.
1075 van Dongen, B.E., Talbot, H.M., Schouten, S., Pearson, P.N., Pancost, R.D., 2006. Well
1076 preserved Palaeogene and Cretaceous biomarkers from the Kilwa area, Tanzania.
1077 Organic Geochemistry 37, 539–557.
1078 van Winden, J.F., Talbot, H.M., Kip, N., Reichart, G.-J., Pol, A., McNamara, N.P., Jetten,
1079 M.S.M., Op den Camp, H.J.M., Sinninghe Damsté, J.S., 2012a. Bacteriohopanepolyol
1080 signatures as markers for methanotrophic bacteria in peat moss. Geochimica et
1081 Cosmochimica Acta 77, 52–61.

van Winden, J.F., Talbot, H.M., De Vleeschouwer, F., Reichart, G.J., Sinninghe Damsté, J.S., 2012b. Variation in methanotroph-related proxies in peat deposits from Misten Bog, Hautes-Fagnes, Belgium. Organic Geochemistry 53, 73-79.

Wagner, T., Kallweit, W., Talbot, H.M., Mollenhauer, G., Boom, A., Zabel, M., 2014. Microbial biomarkers support organic carbon transport from Amazon wetlands to the shelf and deep fan during recent and glacial climate conditions. Organic Geochemistry 67, 85-98.

Wakeham, S.G., Amann, R., Freeman, K.H., Hopmans, E., Jørgensen, B.B., Putnam, I.F., Schouten, S., Sinninghe Damsté, J.S., Talbot, H.M., Woebken, D., 2007. Microbial ecology of the stratified water column of the Black Sea as revealed by a comprehensive biomarker study. Organic Geochemistry 38, 2070-2097.

Watson, D.F., 2002. Environmental Distribution and Sedimentary Fate of Hopanoid Biological Marker Compounds. PhD Thesis, University of Newcastle, UK.

Welander, P.V., Summons, R.E., 2012. Discovery, taxonomic distribution, and phenotypic characterization of a gene required for 3-methylhopanoid production. Proceedings of the National Academy of Science, USA 109, 12905-12910.

Welander, P.V., Hunter, R.C., Zhang, L., Sessions, A.L., Summons, R.E., Newman, D.K., 2009. Hopanoids play a role in membrane integrity and pH homeostasis in *Rhodopseudomonas palustris* TIE-1. Journal of Bacteriology 191, 6145-6156.

Xu, Y., Cooke, M.P., Talbot, H.M., Simpson, M.E., 2009. Bacteriohopanepolyol signatures of bacterial populations in Western Canadian soils. Organic Geochemistry 40, 79–86.

Zhu, C., Talbot, H.M., Wagner, T., Pan, J., Pancost R.D., 2010. Intense aerobic methane oxidation in the Yangtze estuary: A record from 35-aminobacteriohopanepolyols in surface sediments. Organic Geochemistry 41, 1056-1059.

Zhu, C., Talbot, H.M., Wagner, T., Pan, J.-M., Pancost, R.D., 2011. Distribution of hopanoids along a land to sea transect: implications for microbial ecology and the use of hopanoids in environmental studies. Limnology and Oceanography 56, 1850-1865.

Figure legends

Figure 1. (a) Partial APCI mass chromatograms showing base peak ions of individual BHPs which do not contain a nitrogen atom identified via $LCMS^n$. (b) Partial EI mass chromatograms including m/z 191 and 205 fragments (A/B rings) and characteristic D/E +side chain fragments for BHPs identified via GCMS. See appendix for structures. Data from sample depth 11.95 cm (laminated lignite; Table 1).

Figure 2. Partial APCI mass chromatograms showing base peak ions of individual BHPs identified via $LCMS^n$ which contain a nitrogen atom. See appendix for structures. Data from sample depth 115.65 cm (blocky lignite; Table 1.)

Figure 3. EI and APCI MS^2 mass spectra (respectively) of peracetylated derivatives of (a and b) AnhydroBHT, (c and d) proposed "side chain methylated" AnhydroBHT and (e and f) proposed "side chain methylated" 3-methyl-AnhydroBHT (note this compound co elutes with BHT and anhydroBHpentol by GCMS as indicated by the D/E+side chain fragments m/z 493 and 449 respectively; underlined ions in panel e are consistent with the proposed structure). Position of "side-chain methylation" at C-31 in structures shown in parts c-f is tentative (cf. Simonin et al., 1994; Nytoft, 2011). For identification of peaks see Figure 1. Key: Ac = $-COCH_3$; # indicates peak related to aminotriol (**If**; Figure 2). Spectra taken from sample depth 11.95 cm, (laminated lignite, Table 1).

Figure 4. APCI MS^2 spectra of peracetylated derivatives of (a) Aminotriol [**If**], (b) Aminotetrol [**Ig**], (c) Aminopentol [**Ih**], (d) anhydroaminotriol (**Ii**; cf. Eickhoff et al., 2014) (e) proposed 31-oxo-35-aminobacteriohopane-32,33,34-triol [**Ik**] and (f) proposed 32-oxo-35-aminobacteriohopane-33,34 diol [**Ij**]. For identification and relative retention times of peaks see Figure 2. Key: Ac = $-COCH_3$; * indicates loss of 42 Da i.e. partial loss of acetylated OH group as ketene $COCH_2$; (Talbot et al., 2003b); # indicates ions arising from fragmentation of co-eluting parent ion m/z 669, Fig. 1). Data from sample depth 115.65 cm (blocky lignite; Table 1.)

Figure 5. APCI MS^2 and EI mass spectra (respectively) of peracetylated derivatives of (a and b) proposed 31-oxo-bacteriohopane-32,33,34,35-tetrol [**Ie**], (c) APCI MS^2 spectrum of AnhydroBHpentol (isomer i; cf. Talbot et al., 2005) and (d) EI mass spectrum of AnhydroBHpentol (co-eluting with BHT [**Ic**] and "side chain methylated" 3-methly-anhydroBHT [**IIIb**]). For identification of peaks see Figure 1. Data from sample depth 11.95 cm (laminated lignite; Table 1).

Figure 6. Plots of (a) $\delta^{13}C$ values of bulk OM, (b) $\delta^{13}C$ values of C_{29} (circles) and C_{31} (diamonds) hopanes, (c) total biohopanoids as a proportion of total BHPs and (d-h) individual polyfunctionalised biohopanoids as a proportion of total biohopanoids in the Cobham lignite sequence. Open circles indicate 5 samples from within the onset of the CIE (54.4 – 56.6 cm), black circles indicate all other samples. Shaded grey bars indicate clay horizons including lignite with clay laminae in the middle section (Table 1). All isotope data from Pancost et al. (2007) and lithology after Collinson et al. (2003) and Steart et al. (2007).

Figure 7. Plots of (a) $\delta^{13}C$ values of bulk OM, (b) $\delta^{13}C$ values of C_{29} (circles) and C_{31} (diamonds) hopanes, (c) relative abundance of total geohopanoids as % of total BHPs and (d-h) selected known and novel polyfunctionalised hopanoid transformation products as a proportion of total geohopanoids in the Cobham Lignite sequence. Open circles indicate 5 samples from within the onset of the CIE (54.4 – 56.6 cm), black circles indicate all other samples. Shaded grey bars indicate clay horizons including lignite with clay laminae in the middle section (Table 1). All isotope data from Pancost et al. (2007) and lithology from Collinson et al. (2003) and Steart et al. (2007).

Figure 8. Average relative abundance of all BHPs in Cobham lignite sequence (a) blocky lignite [67.5 – 135 cm], (b) clay layer plus uppermost laminated lignite and lowest blocky lignite [57.2-66.8 cm], (c) Onset of carbon isotope excursion [CIE] in laminated lignite [54.45 – 56.6 cm] and (d) lower laminated lignite and sample from sand/mud unit [-1.5 – 54.15 cm].

White bars indicate compounds containing a nitrogen atom, black bars compounds not containing nitrogen. See Appendix for structures.

Table 1. Sample depth in sequence, lithology, bulk carbon isotope ratio values (‰) and relative abundance (%) of individual BHPs from LCMS analysis and biomarker ratios in the Cobham Lignite.

Level	Lithology[a]	δ ^{13}C	Biohopanoids				Polyfunctionalised geohopanoids/Novel products									Ratios	
(cm)		TOC[b]	Ic	If	Ig	Ih	Ia	Ia'	Ib	IIIb	Id	Ie	Ii	Ij	Ik	654/714[e]	If/Ii
135	Blocky Lignite	nm[c]	-[d]	2.8	-	-	60.1	-	11.5	-	4.5	1.9	13.5	5.7	-	5.0	
131.4	Blocky Lignite	-26.82	-	-	-	-	100	-	-	-	-	-	-	-	-		
118.65	Blocky Lignite	-26.93	31.4	23.8	21.1	-	16.3	-	1.8	-	-	-	5.6	-	-	0.4	1.1
115.65	Blocky Lignite	nm	4.1	8.3	4.3	4	41.9	2.3	3.9	0.5	5.2	5.5	8.7	5.3	6	1.2	1.9
102.4	Blocky Lignite	-27.33	1.6	3.6		-	62		7.7	1.3	5	2.7	8.8	4	3.3	2.6	
85.9	Blocky Lignite	-26.14	1.9	3.1	0.3	0.5	60	2.7	8.8	1.8	7.5	3.1	5.8	2.2	2.3	2.0	10.3
75.2	Blocky Lignite	-26.77	1.5	5	1.5	0.7	51.8	-	3.1		2.6	6	14.3	6.3	7.2	3.1	3.3
73.95	Blocky Lignite	-26.82	1.8	5.8	0.4	0	46.2	-	6.2	1.4	5.1	5	17.2	7.5	3.4	3.2	14.5
70.3	Blocky Lignite	nm	1.3	7	2.8	1.5	45.8	-	5.4		1	5.2	14.4	6.1	9.5	2.2	2.5
69.75	Blocky Lignite	nm		6.8	2.1	-	58	-	9.7			3.5	15.9	1.8	2.2	2.5	3.2
69.35	Blocky Lignite	-26.81	1.2	1.2	0.4	0.2	61.3	3.9	9.8	1.7	5.8	6.6	4.5	2.2	1.2	3.9	3.0
68.85	Blocky Lignite	nm	0.7	1.6	0.7	0.2	62.2	4.1	9.6	2.1	5.6	4.4	4.3	1.5	3	2.9	2.3
68.4	Blocky Lignite	nm	1.6	2.1	1	0.2	64.8	4	9.5	2.1	5.2	3.9	4	1.2	0.4	2.1	2.1
67.5	Blocky Lignite	nm	2.6	11.3	13.4	0.6	39.4	4.4	8.9	2.3	4.6	3.4	6.4	1.5	1.2	0.7	0.8
66.8	Blocky Lignite with clay layers	-24.17	7.5	22.6	48.2	-	14.4	-	4.1	0.5	0.7	0.9	1.1	-	-	0.2	0.5
65.3	Clay	-24.83	42.6	29.6	27.8	-	-	-	-	-	-	-	-	-	-	0.2	1.1
58.75	Clay	-25.45	29.1	28.4	33.1	-	6	-	-	-	-	-	3.4	-	-	0.3	0.9
57.2	Laminated Lignite with clay layers	-25.75	14.6	43.1	35.9	-	5.1	-	-	-	-	-	1.3	-	-	0.2	1.2
56.6	Laminated Lignite	-26.97	2	5.2	1.6	0.7	50.3	-	7.6	0.8	6.5	3.7	11.9	5.3	4.4	2.5	3.3
55.9	Laminated Lignite	-26.72	1.2	5.4	0.9	0.8	44.5	-	6	0.7	5.2	3.8	12.6	8	10.9	2.5	6.0
55.3	Laminated Lignite	-27.10	-	5.2	-	-	39.9	-	-	-	-	7.8	29.7	8.6	8.8	5.9	
54.85	Laminated Lignite	-27.16	-	4	0.9	0.8	44.7	-	3.6	-	3	5	15.8	9.5	10.5	4.1	4.4

54.45	Laminated Lignite	-27.01	-	2.5		-	42.4	-	-	-	-	-	26	17.9	11.2	10.7	
54.15	Laminated Lignite	-26.01	-	11.7	5.3	-	70.8	-	-	-	-	-	12.2	-	-	1.2	2.2
43.3	Laminated Lignite	-25.51	1.4	14.2	4.8	-	43.7	-	6.8	0.6	1.7	2.1	20.4	3.1	1.2	1.6	3.0
42.4	Laminated Lignite	-25.20	32.9	-	-	-	50	-	-	-	-	-	17.1	-	-		
41.5	Laminated Lignite	-26.01	1.2	9.3	1.5	-	52.7	-	4.9	1.5	1.6	1.6	19.8	3.8	2.1	2.3	6.2
40.65	Laminated Lignite	-25.28	-	8.3	-	-	45.9	-	-	-	-	-	45.8	-	-	5.7	
39.8	Laminated Lignite	-26.10	1.5	10.1	0.9	-	53.5	-	6.1		5.7	1.5	17.6	2.4	0.7	1.9	11.2
36.1	Laminated Lignite	-25.21	-	7.3	0.6	-	44.4	-	8.3	1.4	5.1	1.9	22.5	5.9	2.6	3.3	12.2
23.05	Laminated Lignite	-25.62	2.9	4.1	0.5	0.6	66.5	2.6	8.6	1.1		2.9	7.3	2	0.9	2.0	8.2
16.5	Laminated Lignite	-25.83	2.1	4.2	0.5	0.2	59.9	2.3	10.6	1.3	4.4	4.4	7.5	2.1	0.5	2.0	8.4
11.95	Laminated Lignite	-26.41	1.8	2.5	0.1	-	60.3	3.5	12.6	1.9	4.6	3.5	7.6	1.4	0.2	3.2	25.0
4.65	Laminated Lignite	-24.77	4.5	1.8	14.3	-	56.5	3.3	9.7	1.2	4.2	3	0.7	0.8	-	0.6	0.1
-1.5	Sand/mud	-25.62	9.6	7.3	20.4	-	45.5	-	10	3.5	2.7	-	1	-	-	0.3	0.4

[a] Detailed description of the lithologies can be found in Collinson et al. (2003) and Steart et al. (2007)

[b] Values from Pancost et al. (2007)

[c] nm =not measured

[d] - indicates compound below detection limit.

[e] ratio calculated from raw peak area before adjustment of the anhydroaminotriol value (see section 2.3).

Appendix 1.

Structures referred to throughout the text and common abbreviated names.

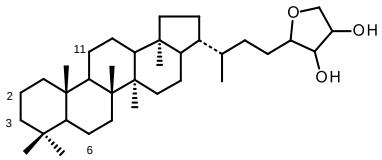

Ia
AnhydroBHT

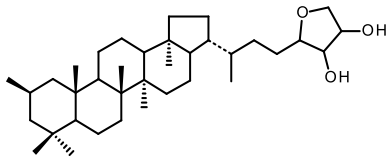

IIa
2-methyl-AnhydroBHT

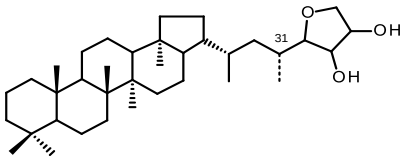

Ib
31-methyl-AnhydroBHT[a]

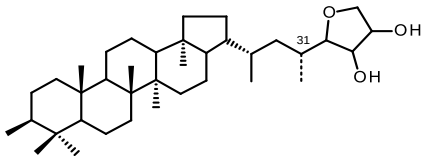

IIIb
3,31-methyl-AnhydroBHT[a]

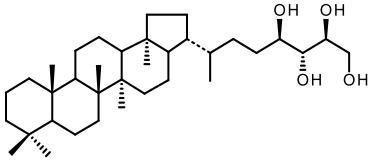

Ic
Bacteriohopanetetrol (BHT)

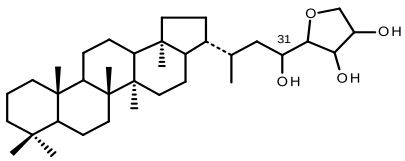

Id
AnhydroBHpentol

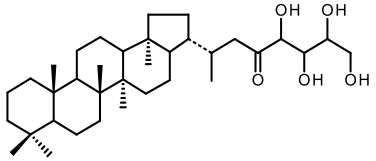

Ie
31-oxo-BHT[b]

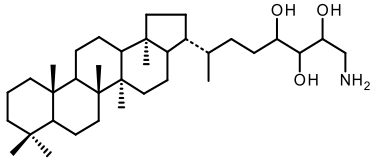

If
Aminotriol

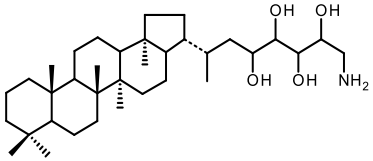

Ig
Aminotetrol

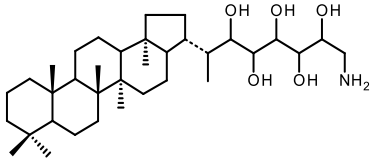

Ih
Aminopentol

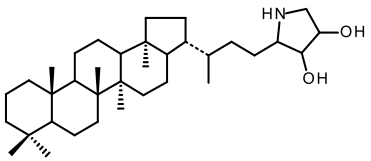

Ii
Anhydroaminotriol

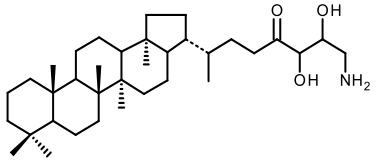

Ij
32-oxo-35-Aminodiol[b]

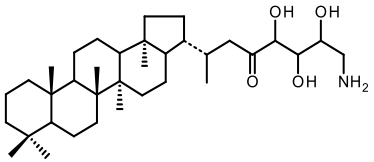

Ik
31-oxo-35-Aminotriol[b]

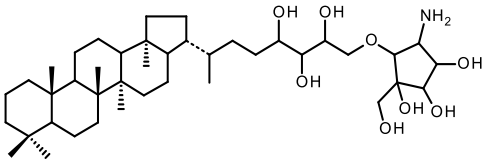

Im
BHT cyclitol ether

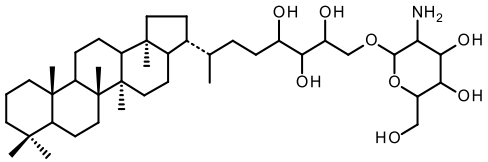

In
BHT glucosamine

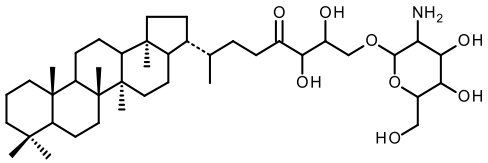

Io
32-oxo-bateriohopanetriol glucosamine

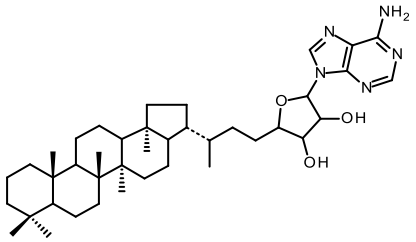

Ip
Adenosylhopane

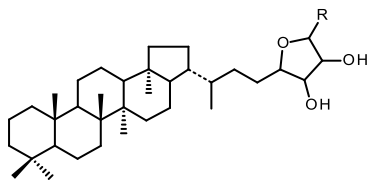

Iq
Adenosylhopane-type[c]
(R = unknown)

[a] position of methylation at C-31 is tentative but limited to the side chain based on EI spectra (Fig. 3) and indicated at C-31 based on previous studies (Simonin et al., 1994; Nytoft, 2011)

[b] location of ketone is tentative but is limited to the side chain in **Ie** based on EI spectrum (Fig. 5)

[c] terminal group structure (R) unknown but can be differentiated from **Ip** based on APCI base peak ion and MS^2 spectrum (Cooke et al., 2008a; Rethemeyer et al., 2010).

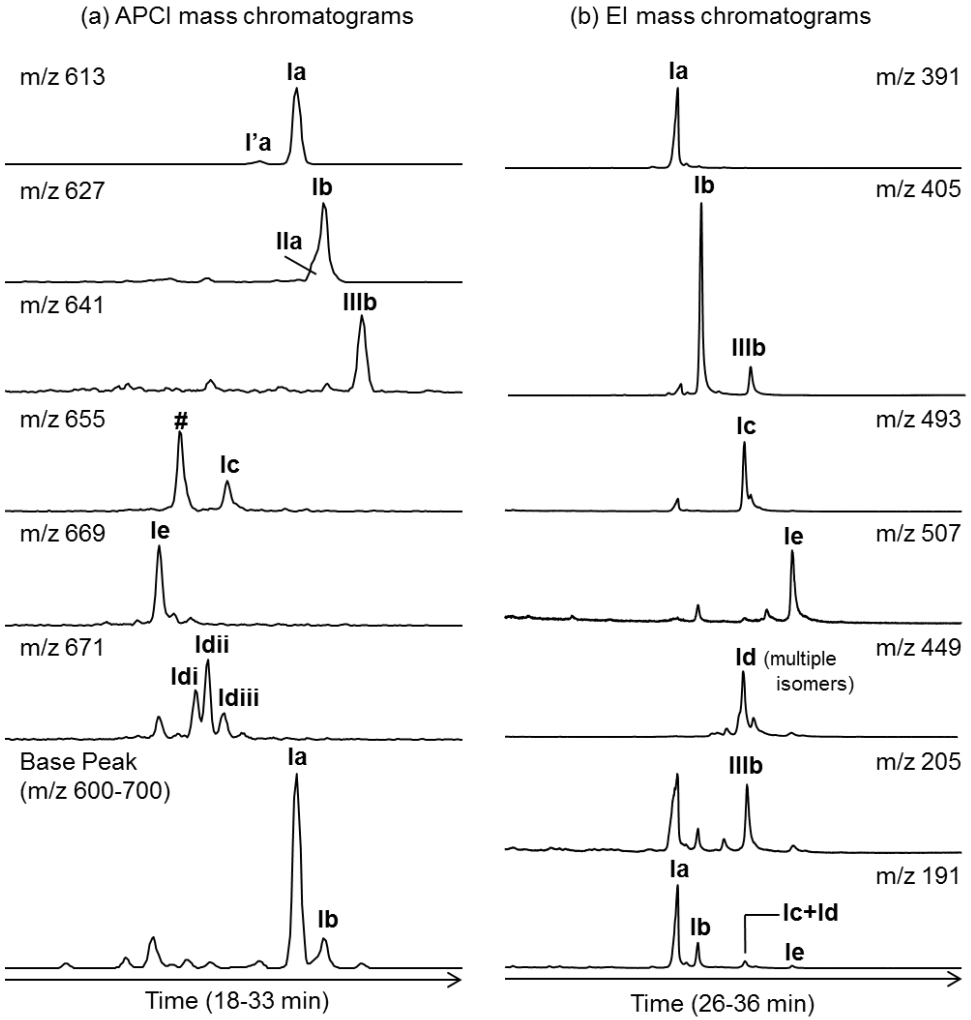
(a) APCI mass chromatograms
(b) EI mass chromatograms
m/z 613
Ia
I'a
m/z 627
Ib
IIa
m/z 641
IIIb
m/z 655
#
Ic
m/z 669
Ie
m/z 671
Idii
Idi
Idiii
Base Peak
(m/z 600-700)
Ia
Ib
Time (18-33 min)
Ia
m/z 391
Ib
m/z 405
IIIb
m/z 493
Ic
m/z 507
Ie
m/z 449
Id (multiple isomers)
m/z 205
IIIb
m/z 191
Ia
Ib
Ic+Id
Ie
Time (26-36 min)

Figure 1

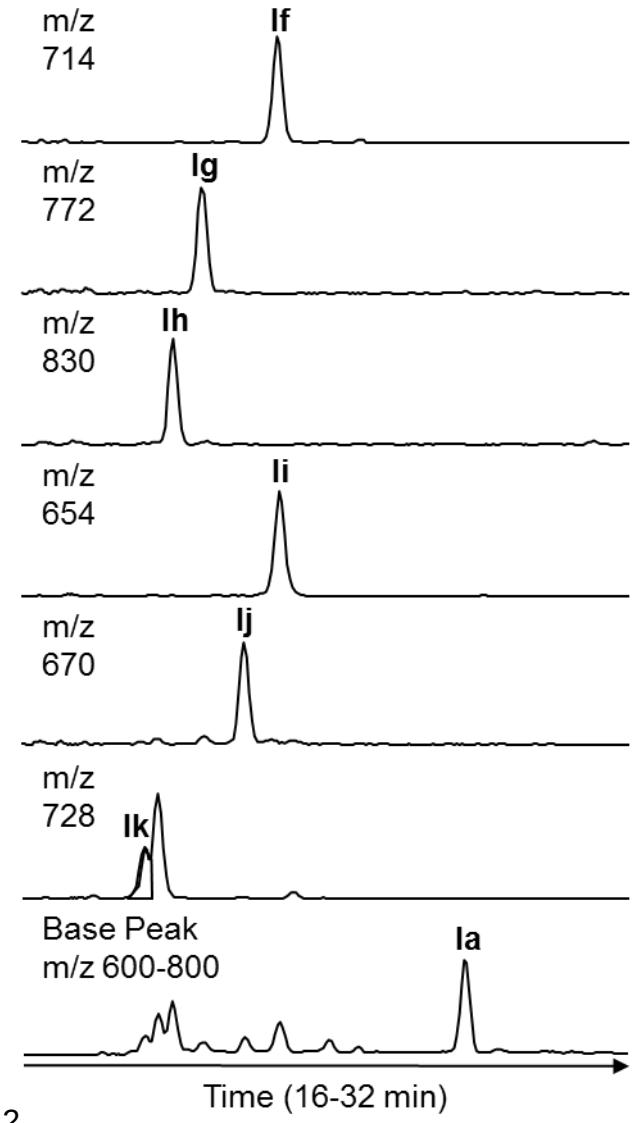

1189 Figure 2

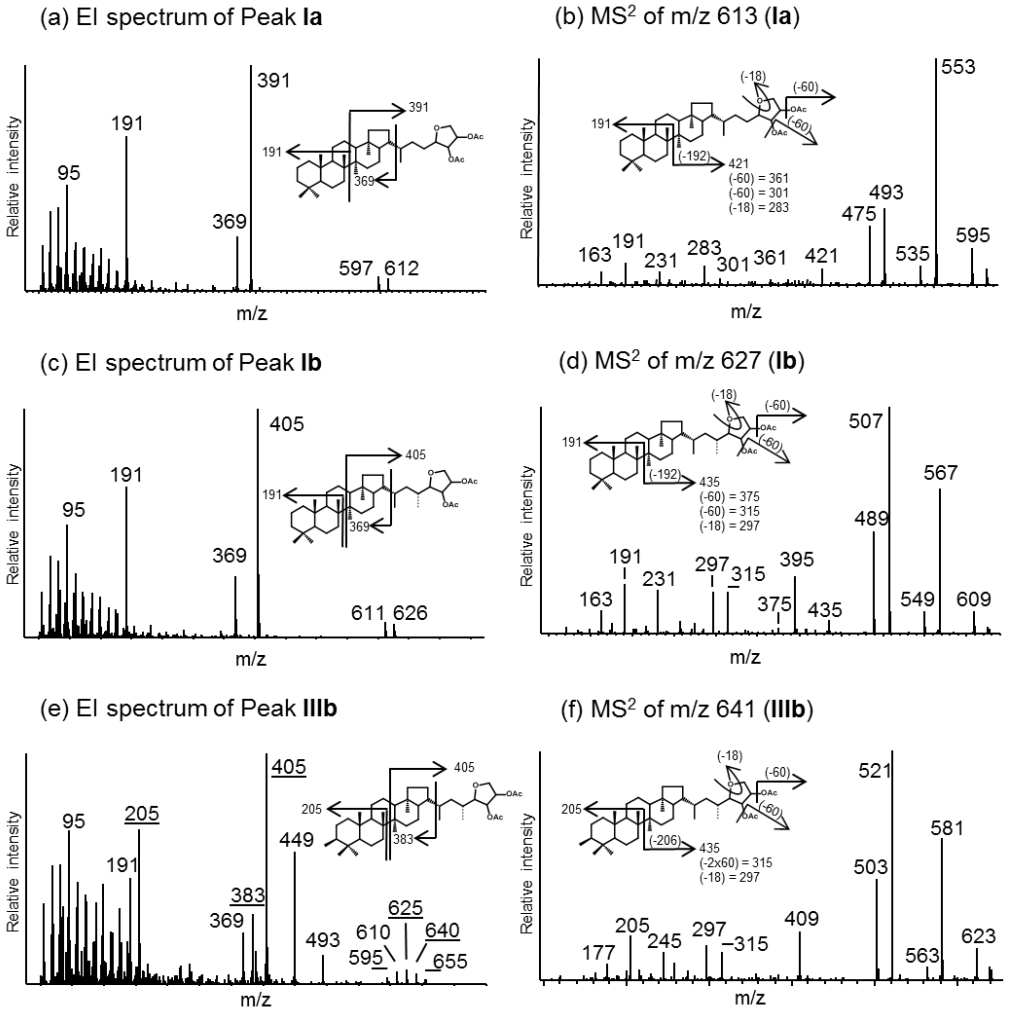
(a) EI spectrum of Peak **Ia**
(b) MS^2 of m/z 613 (**Ia**)
(c) EI spectrum of Peak **Ib**
(d) MS^2 of m/z 627 (**Ib**)
(e) EI spectrum of Peak **IIIb**
(f) MS^2 of m/z 641 (**IIIb**)
Relative intensity
m/z

Figure 3.

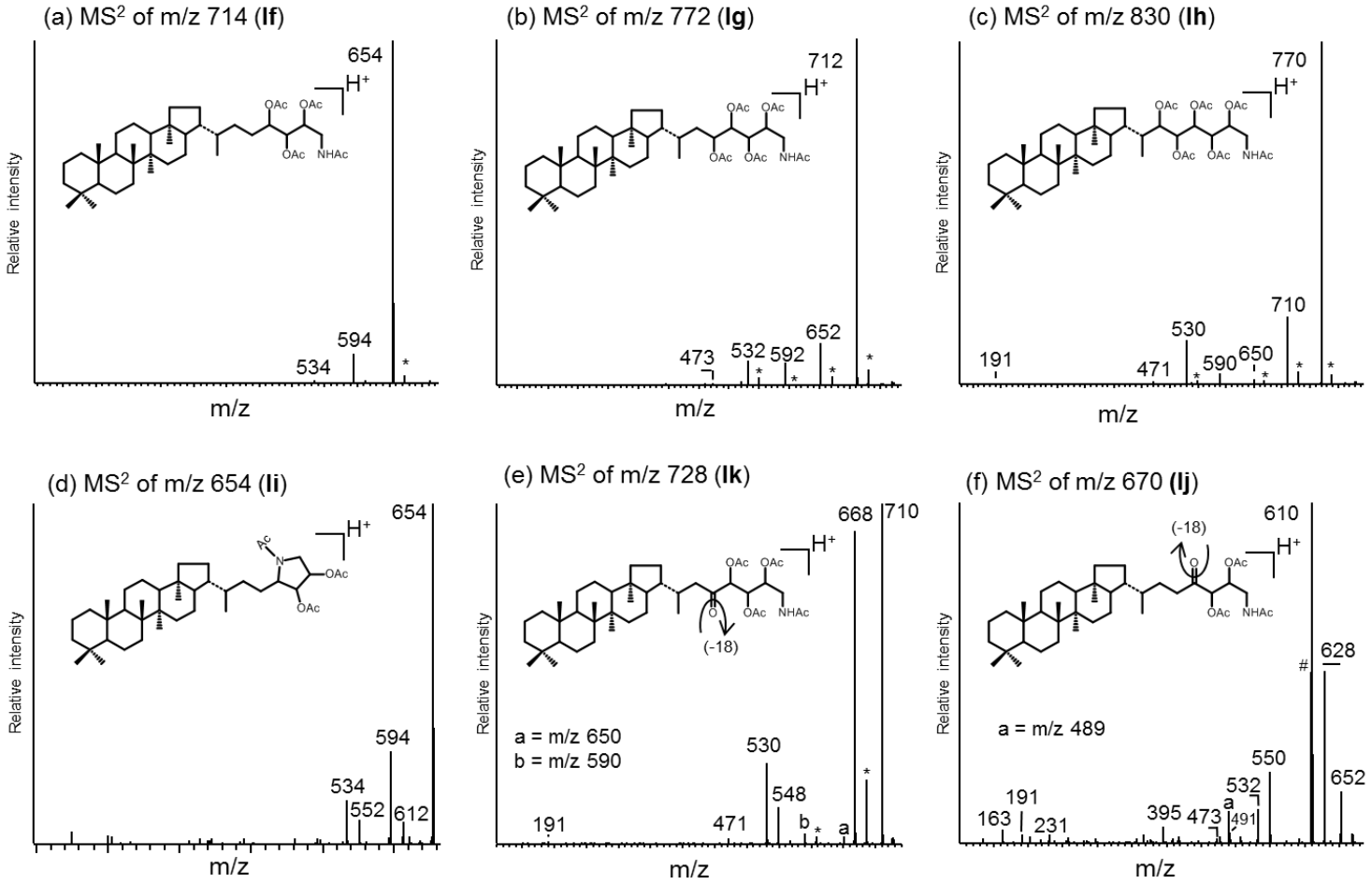
(a) MS2 of m/z 714 (If)
654
H+
OAc OAc
OAc NHAc
Relative intensity
594
534
*
m/z
(b) MS2 of m/z 772 (Ig)
712
H+
OAc OAc
OAc OAc NHAc
Relative intensity
652
473
532
592
*
m/z
(c) MS2 of m/z 830 (Ih)
770
H+
OAc OAc OAc
OAc OAc NHAc
Relative intensity
710
530
191
471
590
650
*
m/z
(d) MS2 of m/z 654 (Ii)
654
H+
Ac
N
OAc
OAc
Relative intensity
594
534
552
612
m/z
(e) MS2 of m/z 728 (Ik)
668
710
H+
OAc OAc
O
OAc NHAc
(-18)
Relative intensity
a = m/z 650
b = m/z 590
530
548
191
471
b
a
*
m/z
(f) MS2 of m/z 670 (Ij)
610
(-18)
H+
O
OAc
OAc NHAc
Relative intensity
#
628
a = m/z 489
550
532
652
191
163
231
395
473
a
491
m/z

Figure 4.

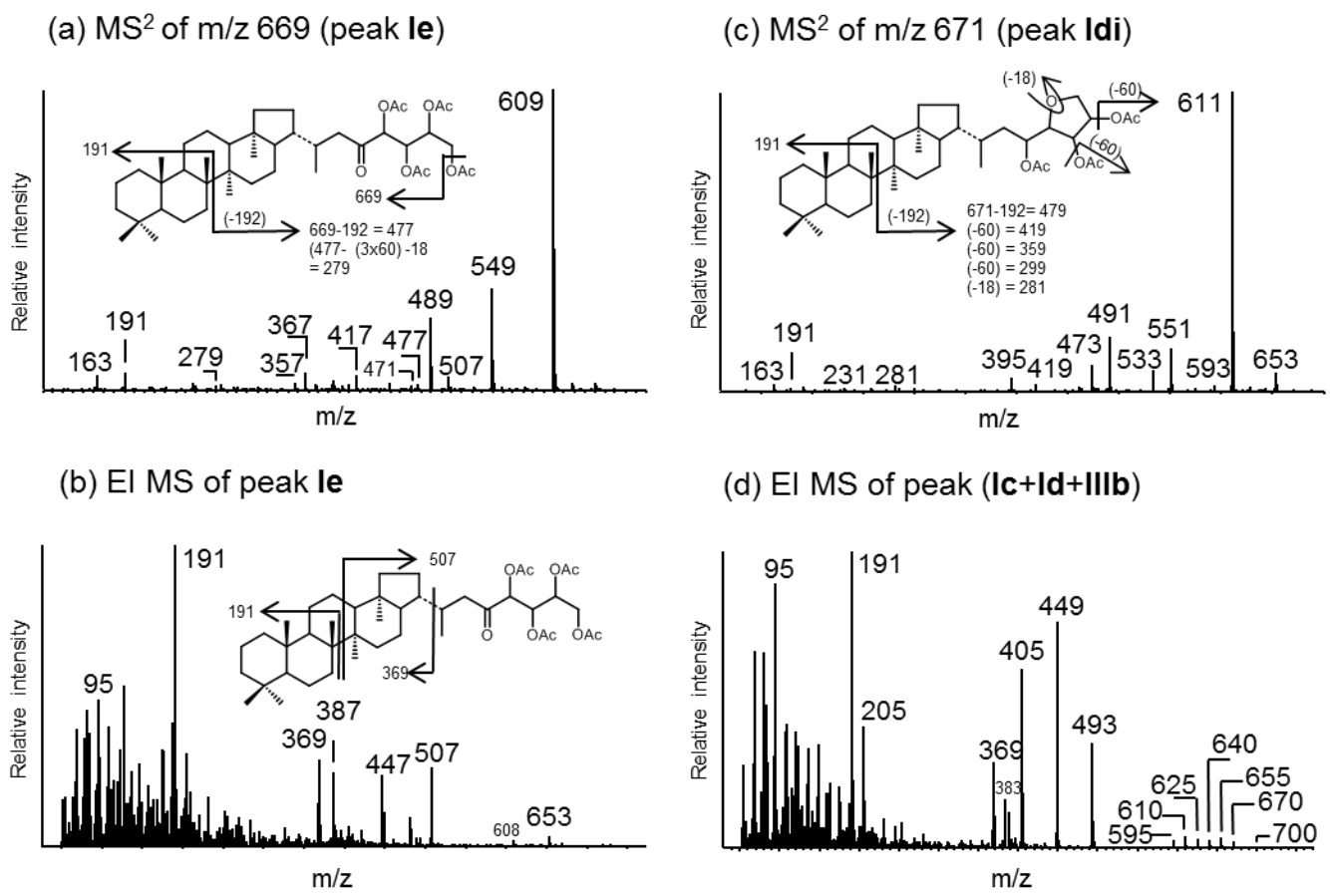
(a) MS2 of m/z 669 (peak **Ie**)
Relative intensity
m/z
191
163
279
357
367
417
471
477
507
489
549
609
669
(-192)
669-192 = 477
(477- (3x60) -18
= 279
OAc
(c) MS2 of m/z 671 (peak **Idi**)
191
163
231 281
395
419
473
491
533
551
593
653
611
(-18)
(-60)
671-192= 479
(-60) = 419
(-60) = 359
(-60) = 299
(-18) = 281
(b) EI MS of peak **Ie**
95
191
369
387
447
507
608
653
(d) EI MS of peak (**Ic**+**Id**+**IIIb**)
95
191
205
369
383
405
449
493
595
610
625
640
655
670
700

Figure 5.

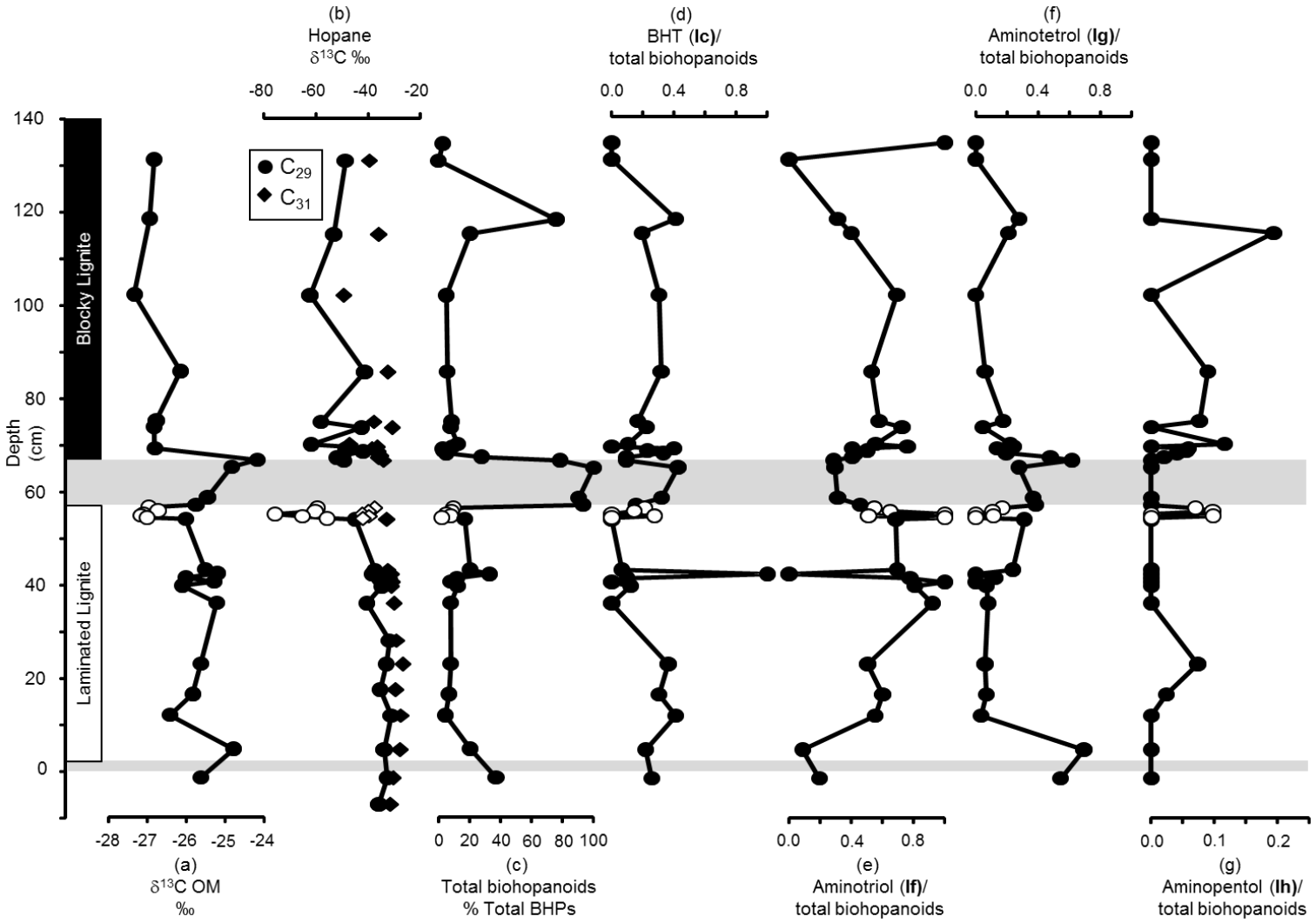

1200

1201 Figure 6.

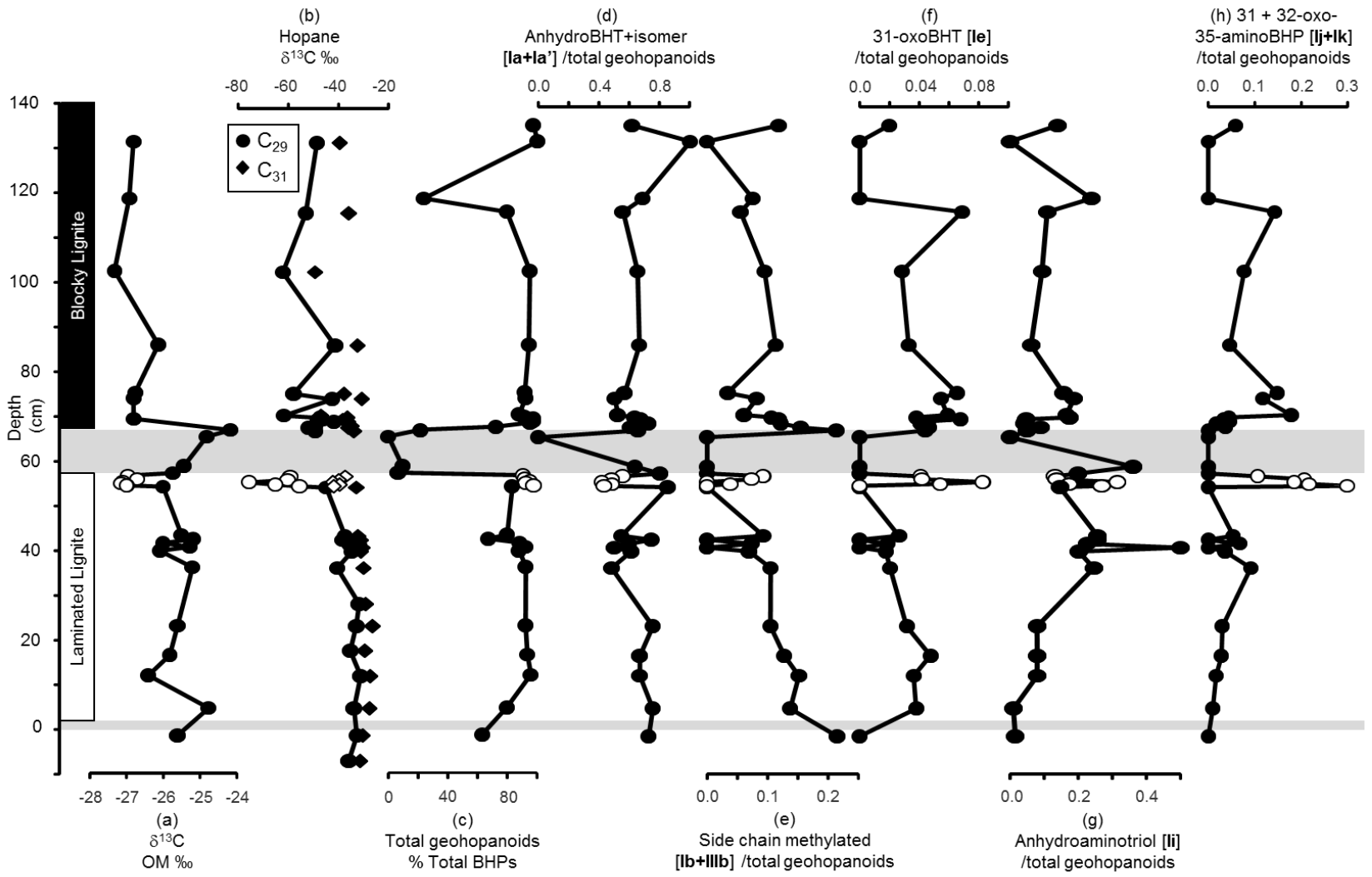

1202

1203 Figure 7.

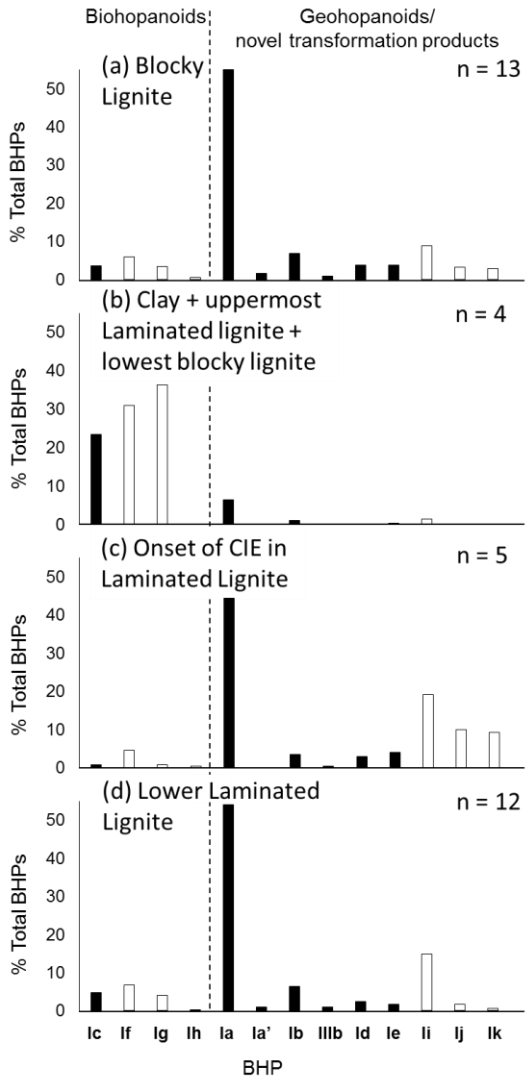
Biohopanoids
Geohopanoids/
novel transformation products
(a) Blocky
Lignite
n = 13
(b) Clay + uppermost
Laminated lignite +
lowest blocky lignite
n = 4
(c) Onset of CIE in
Laminated Lignite
n = 5
(d) Lower Laminated
Lignite
n = 12
% Total BHPs
0
10
20
30
40
50
Ic
If
Ig
Ih
Ia
Ia'
Ib
IIIb
Id
Ie
Ii
Ij
Ik
BHP

Figure 8.